Fermilab FERMILAB-Pub-97/352-E

Measurement of B Hadron Lifetimes Using J/ψ Final States at CDF

F. Abe,[17] H. Akimoto,[39] A. Akopian,[31] M. G. Albrow,[7] A. Amadon,[5] S. R. Amendolia,[27] D. Amidei,[20] J. Antos,[33] S. Aota,[37] G. Apollinari,[31] T. Arisawa,[39] T. Asakawa,[37] W. Ashmanskas,[18] M. Atac,[7] F. Azfar,[26] P. Azzi-Bacchetta,[25] N. Bacchetta,[25] S. Bagdasarov,[31] M. W. Bailey,[22] P. de Barbaro,[30] A. Barbaro-Galtieri,[18] V. E. Barnes,[29] B. A. Barnett,[15] M. Barone,[9] G. Bauer,[19] T. Baumann,[11] F. Bedeschi,[27] S. Behrends,[3] S. Belforte,[27] G. Bellettini,[27] J. Bellinger,[40] D. Benjamin,[35] J. Bensinger,[3] A. Beretvas,[7] J. P. Berge,[7] J. Berryhill,[5] S. Bertolucci,[9] S. Bettelli,[27] B. Bevensee,[26] A. Bhatti,[31] K. Biery,[7] C. Bigongiari,[27] M. Binkley,[7] D. Bisello,[25] R. E. Blair,[1] C. Blocker,[3] S. Blusk,[30] A. Bodek,[30] W. Bokhari,[26] G. Bolla,[29] Y. Bonushkin,[4] D. Bortoletto,[29] J. Boudreau,[28] L. Breccia,[2] C. Bromberg,[21] N. Bruner,[22] R. Brunetti,[2] E. Buckley-Geer,[7] H. S. Budd,[30] K. Burkett,[20] G. Busetto,[25] A. Byon-Wagner,[7] K. L. Byrum,[1] J. Cammerata,[29] M. Campbell,[20] A. Caner,[27] W. Carithers,[18] D. Carlsmith,[40] J. Cassada,[30] A. Castro,[25] D. Cauz,[36] A. Cerri,[27] P. S. Chang,[33] P. T. Chang,[33] H. Y. Chao,[33] J. Chapman,[20] M. -T. Cheng,[33] M. Chertok,[34] G. Chiarelli,[27] C. N. Chiou,[33] L. Christofek,[13] M. L. Chu,[33] S. Cihangir,[7] A. G. Clark,[10] M. Cobal,[27] E. Cocca,[27] M. Contreras,[5] J. Conway,[32] J. Cooper,[7] M. Cordelli,[9] D. Costanzo,[27] C. Couyoumtzelis,[10] D. Cronin-Hennessy,[6] R. Culbertson,[5] D. Dagenhart,[38] T. Daniels,[19] F. DeJongh,[7] S. Dell'Agnello,[9] M. Dell'Orso,[27] R. Demina,[7] L. Demortier,[31] M. Deninno,[2] P. F. Derwent,[7] T. Devlin,[32] J. R. Dittmann,[6] S. Donati,[27] J. Done,[34] T. Dorigo,[25] N. Eddy,[20] K. Einsweiler,[18] J. E. Elias,[7] R. Ely,[18] E. Engels, Jr.,[28] W. Erdmann,[7] D. Errede,[13] S. Errede,[13] Q. Fan,[30] R. G. Feild,[41] Z. Feng,[15] C. Ferretti,[27] I. Fiori,[2] B. Flaugher,[7] G. W. Foster,[7] M. Franklin,[11] J. Freeman,[7] J. Friedman,[19] H. Frisch,[5] Y. Fukui,[17] S. Gadomski,[14] S. Galeotti,[27] M. Gallinaro,[26] O. Ganel,[35] M. Garcia-Sciveres,[18] A. F. Garfinkel,[29] C. Gay,[41] S. Geer,[7] D. W. Gerdes,[15] P. Giannetti,[27] N. Giokaris,[31] P. Giromini,[9] G. Giusti,[27] M. Gold,[22] A. Gordon,[11] A. T. Goshaw,[6] Y. Gotra,[25] K. Goulianos,[31] H. Grassmann,[36] L. Groer,[32] C. Grosso-Pilcher,[5] G. Guillian,[20] J. Guimaraes da Costa,[15] R. S. Guo,[33] C. Haber,[18] E. Hafen,[19] S. R. Hahn,[7] R. Hamilton,[11] T. Handa,[12] R. Handler,[40] F. Happacher,[9] K. Hara,[37] A. D. Hardman,[29] R. M. Harris,[7] F. Hartmann,[16] J. Hauser,[4] E. Hayashi,[37] J. Heinrich,[26] W. Hao,[35] B. Hinrichsen,[14] K. D. Hoffman,[29] M. Hohlmann,[5] C. Holck,[26] R. Hollebeek,[26] L. Holloway,[13] Z. Huang,[20] B. T. Huffman,[28] R. Hughes,[23] J. Huston,[21] J. Huth,[11] H. Ikeda,[37] M. Incagli,[27] J. Incandela,[7] G. Introzzi,[27] J. Iwai,[39] Y. Iwata,[12] E. James,[20] H. Jensen,[7] U. Joshi,[7] E. Kajfasz,[25] H. Kambara,[10] T. Kamon,[34] T. Kaneko,[37] K. Karr,[38] H. Kasha,[41] Y. Kato,[24] T. A. Keaffaber,[29] K. Kelley,[19] R. D. Kennedy,[7] R. Kephart,[7] D. Kestenbaum,[11] D. Khazins,[6] T. Kikuchi,[37] B. J. Kim,[27] H. S. Kim,[14] S. H. Kim,[37] Y. K. Kim,[18] L. Kirsch,[3] S. Klimenko,[8] D. Knoblauch,[16] P. Koehn,[23] A. Köngeter,[16] K. Kondo,[37] J. Konigsberg,[8] K. Kordas,[14] A. Korytov,[8] E. Kovacs,[1] W. Kowald,[6] J. Kroll,[26] M. Kruse,[30] S. E. Kuhlmann,[1] E. Kuns,[32] K. Kurino,[12] T. Kuwabara,[37] A. T. Laasanen,[29] I. Nakano,[12] S. Lami,[27] S. Lammel,[7] J. I. Lamoureux,[3] M. Lancaster,[18] M. Lanzoni,[27] G. Latino,[27] T. LeCompte,[1] S. Leone,[27] J. D. Lewis,[7] P. Limon,[7] M. Lindgren,[4] T. M. Liss,[13] J. B. Liu,[30] Y. C. Liu,[33] N. Lockyer,[26] O. Long,[26] C. Loomis,[32] M. Loreti,[25] D. Lucchesi,[27] P. Lukens,[7] S. Lusin,[40] J. Lys,[18] K. Maeshima,[7] P. Maksimovic,[19] M. Mangano,[27] M. Mariotti,[25] J. P. Marriner,[7] A. Martin,[41] J. A. J. Matthews,[22] P. Mazzanti,[2] P. McIntyre,[34] P. Melese,[31] M. Menguzzato,[25] A. Menzione,[27] E. Meschi,[27] S. Metzler,[26] C. Miao,[20] T. Miao,[7] G. Michail,[11] R. Miller,[21] H. Minato,[37] S. Miscetti,[9] M. Mishina,[17] S. Miyashita,[37] N. Moggi,[27] E. Moore,[22] Y. Morita,[17] A. Mukherjee,[7] T. Muller,[16] P. Murat,[27] S. Murgia,[21] H. Nakada,[37] I. Nakano,[12] C. Nelson,[7] D. Neuberger,[16] C. Newman-Holmes,[7] C.-Y. P. Ngan,[19] L. Nodulman,[1] S. H. Oh,[6] T. Ohmoto,[12] T. Ohsugi,[12] R. Oishi,[37] M. Okabe,[37] T. Okusawa,[24] J. Olsen,[40] C. Pagliarone,[27] R. Paoletti,[27] V. Papadimitriou,[35] S. P. Pappas,[41] N. Parashar,[27] A. Parri,[9] J. Patrick,[7] G. Pauletta,[36] M. Paulini,[18] A. Perazzo,[27] L. Pescara,[25] M. D. Peters,[18] T. J. Phillips,[6] G. Piacentino,[27] M. Pillai,[30] K. T. Pitts,[7] R. Plunkett,[7] L. Pondrom,[40] J. Proudfoot,[1] F. Ptohos,[11] G. Punzi,[27] K. Ragan,[14] D. Reher,[18] M. Reischl,[16] A. Ribon,[25] F. Rimondi,[2] L. Ristori,[27] W. J. Robertson,[6] T. Rodrigo,[27] S. Rolli,[38] L. Rosenson,[19] R. Roser,[13] T. Saab,[14] W. K. Sakumoto,[30] D. Saltzberg,[4] A. Sansoni,[9] L. Santi,[36] H. Sato,[37] P. Schlabach,[7] E. E. Schmidt,[7] M. P. Schmidt,[41] A. Scott,[4] A. Scribano,[27] S. Segler,[7] S. Seidel,[22] Y. Seiya,[37] F. Semeria,[2] T. Shah,[19] M. D. Shapiro,[18] N. M. Shaw,[29] P. F. Shepard,[28] T. Shibayama,[37] M. Shimojima,[37] M. Shochet,[5] J. Siegrist,[18] A. Sill,[35] P. Sinervo,[14] P. Singh,[13] J. Skarha,[29] K. Sliwa,[38] C. Smith,[15] F. D. Snider,[15] J. Spalding,[7] T. Speer,[10] P. Sphicas,[19] F. Spinella,[27] M. Spiropulu,[11] L. Spiegel,[7] L. Stanco,[25] J. Steele,[40] A. Stefanini,[27] R. Ströhmer,[7a] J. Strologas,[13] F. Strumia, [10] D. Stuart,[7] K. Sumorok,[19] J. Suzuki,[37] T. Suzuki,[37] T. Takahashi,[24] T. Takano,[24] R. Takashima,[12] K. Takikawa,[37] M. Tanaka,[37] B. Tannenbaum,[22] F. Tartarelli,[27] W. Taylor,[14] M. Tecchio,[20] P. K. Teng,[33] Y. Teramoto,[24] K. Terashi,[37] S. Tether,[19] D. Theriot,[7] T. L. Thomas,[22] R. Thurman-Keup,[1] M. Timko,[38] P. Tipton,[30] A. Titov,[31] S. Tkaczyk,[7] D. Toback,[5] K. Tollefson,[19] A. Tollestrup,[7] H. Toyoda,[24] W. Trischuk,[14] J. F. de Troconiz,[11] S. Truitt,[20] J. Tseng,[19] N. Turini,[27] T. Uchida,[37] F. Ukegawa,[26] J. Valls,[32] S. C. van den Brink,[28] S. Vejcik, III,[20] G. Velev,[27] R. Vidal,[7] R. Vilar,[7a] D. Vucinic,[19] R. G. Wagner,[1] R. L. Wagner,[7] J. Wahl,[5] N. B. Wallace,[27] A. M. Walsh,[32] C. Wang,[6] C. H. Wang,[33] M. J. Wang,[33] A. Warburton,[14] T. Watanabe,[37] T. Watts,[32] R. Webb,[34] C. Wei,[6] H. Wenzel,[16] W. C. Wester, III,[7] A. B. Wicklund,[1] E. Wicklund,[7] R. Wilkinson,[26] H. H. Williams,[26] P. Wilson,[5] B. L. Winer,[23] D. Winn,[20] D. Wolinski,[20] J. Wolinski,[21] S. Worm,[22] X. Wu,[10] J. Wyss,[27] A. Yagil,[7] W. Yao,[18] K. Yasuoka,[37] G. P. Yeh,[7] P. Yeh,[33] J. Yoh,[7] C. Yosef,[21] T. Yoshida,[24] I. Yu,[7] A. Zanetti,[36]

F. Zetti,[27] and S. Zucchelli[2]

(CDF Collaboration)

[1] *Argonne National Laboratory, Argonne, Illinois 60439*
[2] *Istituto Nazionale di Fisica Nucleare, University of Bologna, I-40127 Bologna, Italy*
[3] *Brandeis University, Waltham, Massachusetts 02254*
[4] *University of California at Los Angeles, Los Angeles, California 90024*
[5] *University of Chicago, Chicago, Illinois 60637*
[6] *Duke University, Durham, North Carolina 27708*
[7] *Fermi National Accelerator Laboratory, Batavia, Illinois 60510*
[8] *University of Florida, Gainesville, FL 32611*
[9] *Laboratori Nazionali di Frascati, Istituto Nazionale di Fisica Nucleare, I-00044 Frascati, Italy*
[10] *University of Geneva, CH-1211 Geneva 4, Switzerland*
[11] *Harvard University, Cambridge, Massachusetts 02138*
[12] *Hiroshima University, Higashi-Hiroshima 724, Japan*
[13] *University of Illinois, Urbana, Illinois 61801*
[14] *Institute of Particle Physics, McGill University, Montreal H3A 2T8, and University of Toronto, Toronto M5S 1A7, Canada*
[15] *The Johns Hopkins University, Baltimore, Maryland 21218*
[16] *Institut für Experimentelle Kernphysik, Universität Karlsruhe, 76128 Karlsruhe, Germany*
[17] *National Laboratory for High Energy Physics (KEK), Tsukuba, Ibaraki 305, Japan*
[18] *Ernest Orlando Lawrence Berkeley National Laboratory, Berkeley, California 94720*
[19] *Massachusetts Institute of Technology, Cambridge, Massachusetts 02139*
[20] *University of Michigan, Ann Arbor, Michigan 48109*
[21] *Michigan State University, East Lansing, Michigan 48824*
[22] *University of New Mexico, Albuquerque, New Mexico 87131*
[23] *The Ohio State University, Columbus, OH 43210*
[24] *Osaka City University, Osaka 588, Japan*
[25] *Universita di Padova, Istituto Nazionale di Fisica Nucleare, Sezione di Padova, I-35131 Padova, Italy*
[26] *University of Pennsylvania, Philadelphia, Pennsylvania 19104*
[27] *Istituto Nazionale di Fisica Nucleare, University and Scuola Normale Superiore of Pisa, I-56100 Pisa, Italy*
[28] *University of Pittsburgh, Pittsburgh, Pennsylvania 15260*
[29] *Purdue University, West Lafayette, Indiana 47907*
[30] *University of Rochester, Rochester, New York 14627*
[31] *Rockefeller University, New York, New York 10021*
[32] *Rutgers University, Piscataway, New Jersey 08855*
[33] *Academia Sinica, Taipei, Taiwan 11530, Republic of China*
[34] *Texas A&M University, College Station, Texas 77843*
[35] *Texas Tech University, Lubbock, Texas 79409*
[36] *Istituto Nazionale di Fisica Nucleare, University of Trieste/ Udine, Italy*
[37] *University of Tsukuba, Tsukuba, Ibaraki 315, Japan*
[38] *Tufts University, Medford, Massachusetts 02155*
[39] *Waseda University, Tokyo 169, Japan*
[40] *University of Wisconsin, Madison, Wisconsin 53706*
[41] *Yale University, New Haven, Connecticut 06520*

The average Bottom-hadron and individual B^+, B^0, and B_s^0 meson lifetimes have been determined using decays with a $J/\psi \to \mu^+\mu^-$ in the final state. The data sample consists of 110 pb^{-1} of $\overline{p}p$ collisions at $\sqrt{s} = 1.8$ TeV collected by the CDF detector at the Fermilab Tevatron collider during 1992-1995. For the average lifetime of B-hadrons decaying into J/ψ+X, we obtain $\langle \tau_b \rangle = 1.533 \pm 0.015(\text{stat}) \, ^{+0.035}_{-0.031}$ (syst) ps. For the B^+ and B^0 meson lifetimes, we determine $\tau(B^+) = 1.68 \pm 0.07$ (stat) $\pm$ 0.02 (syst) ps, $\tau(B^0) = 1.58 \pm 0.09$ (stat) $\pm$ 0.02 (syst) ps, and $\tau(B^+)/\tau(B^0) = 1.06 \pm 0.07$ (stat) $\pm$ 0.02 (syst). For the B_s^0 meson lifetime, we find $\tau(B_s^0) = 1.34^{+0.23}_{-0.19}$ (stat) $\pm$ 0.05 (syst)ps.

PACS numbers:13.25.Hw , 14.40.Nd

I. INTRODUCTION

The precise determination of the specific B lifetimes is important for the determination of elements of the Cabibbo-Kobayashi-Maskawa matrix. Furthermore measurements of the lifetimes of B-hadrons probe decay mechanisms beyond the simple spectator quark decay model. Lifetime differences can arise from unequal amplitudes for the annihilation and W-exchange diagrams, as well as from final state Pauli interference effects. These mechanisms play an important role in the observed factor of 2.5 in the lifetime difference between the D^+ and D^0 mesons [1]. The lifetime difference between the B^+ and B^0 is expected to be much smaller, on the order of 5-20% [2–4] due to the heavier b-quark mass. The B^0 and B_s^0 meson lifetimes are expected to be nearly identical. The observed value of the Λ_b-baryon lifetime [5] is unexpectedly short.

CDF [6–9] and several e^+e^- experiments have measured the average B-hadron lifetime [10] and the individual B^+, B^0 [11], and B_s^0 [12] meson lifetimes. The measurement precision [13] is now approaching the 5% level. This begins to test the lifetime hierarchy predictions of different theoretical models.

In this paper, we report measurements of the average B-hadron and individual B^+, B^0, and B_s^0 meson lifetimes using events containing a $J/\psi \to \mu^+\mu^-$ decay in the final state. The data sample consists of ≈ 110 pb^{-1} of $p\bar{p}$ collisions at $\sqrt{s} = 1.8$ TeV collected by the CDF detector at the Fermilab Tevatron collider during 1992-1995 (Run 1). Of this, approximately 20 pb^{-1} were collected during the 1992-1993 running period (Run 1A), and approximately 90 pb^{-1} were collected during the 1994-1995 running period (Run 1B). Partially reconstructed $B \to J/\psi X$ events were used for the average B-hadron lifetime. For the B^+ and B^0 meson lifetimes, fully reconstructed $B \to \Psi K$ decays were identified, where $B = B^+$ or B^0, $\Psi = J/\psi$ or $\psi(2S)$, and $K = K^+$, $K^*(892)^+$, K_S^0, or $K^*(892)^0$. For the B_s^0 meson lifetime [14], the exclusive decay mode $B_s^0 \to J/\psi\phi$, $\phi \to K^+K^-$, was reconstructed.

We have organized this paper as follows. First, in Section II we briefly describe the components of the CDF detector relevant to the analyses presented in this paper. In Section III, we describe the data collection and event selection procedures. Section IV covers the reconstruction of exclusive B decays. Sections V and VI describe the determination of the primary interaction vertex and the variables used to extract the lifetime. We present the measurement of the average B-hadron lifetime in Section VII. This is followed by the determination of the individual B^+ and B^0 meson lifetimes in Section VIII and the B_s^0 lifetime in Section IX. In Section X, we summarize our results.

II. THE CDF DETECTOR

The CDF detector is described in [15]. A schematic drawing of one quarter section of CDF is shown in Fig. 1. The polar angle θ in cylindrical coordinates is measured from the proton beam axis (z-axis), and the azimuthal angle ϕ from the plane of the Tevatron. Throughout this paper 'transverse plane' refers to the plane normal to the proton beam (r-ϕ-plane). The detector components most relevant to the measurements reported in this paper are the muon chambers and the charged particle tracking system.

The tracking system consists of three detectors in a 1.4 T magnetic field generated by a superconducting solenoid of length 4.8 m and radius 1.5 m. The innermost tracking device is a silicon microstrip vertex detector (SVX) [16], which provides spatial measurements in the r-ϕ plane. The SVX active region is 51 cm long and consists of two cylindrical barrels, separated by a gap of 2.15 cm at the center of the detector. The $p\bar{p}$ collision vertices are Gaussian-distributed along the beamline with $\sigma \approx 30$ cm (see Section V), therefore only about 60% of all $J/\psi \to \mu^+\mu^-$ events have both muon tracks reconstructed in the SVX. Each barrel consists of four layers of silicon strip detectors with 60 μm pitch between readout strips for the three inner layers and 55 μm pitch for the fourth layer. The layers are located at radii between 3.0 and 7.9 cm from the beam line. The impact parameter resolution of the SVX is $\sigma_D(p_T) = (13 + 40/p_T)$ μm [16], where p_T is the transverse momentum of the track in GeV/c. The track impact parameter D is defined as the as the distance of closest approach of the track helix to the beam axis measured in the plane perpendicular to the beam.

Outside the SVX is a set of time projection chambers (VTX) which measure the position of the primary interaction vertex along the z-axis. The central tracking chamber (CTC) is a 3m long cylindrical drift chamber with inner and outer radii of 0.3 and 1.3 m and covering the pseudorapidity interval $|\eta| < 1.1$, where $\eta = -\ln(\tan(\theta/2))$. The CTC contains 84 layers grouped into nine alternating super-layers of axial (12 layers each) and stereo wires (6 layers each). Combined, the CTC and SVX provide a transverse momentum resolution of $\delta p_T/p_T \sim \sqrt{(0.9p_T)^2 + (6.6)^2} \times 10^{-3}$, where p_T is in GeV/c.

The central muon system consisting of three components (CMU,CMP and CMX) is capable of detecting muons with $p_T \geq 1.4$ GeV/c in the pseudorapidity interval $|\eta| < 1.0$. The CMU system covers the region $|\eta| < 0.6$ and consists of 4 layers of planar drift chambers outside the hadron calorimeter allowing the reconstruction of track segments for particles penetrating the 5 absorption lengths of material (at normal incidence). Outside the CMU there is an additional absorber of 60 cm of steel followed by 4 layers of drift chambers (CM-

P). Finally the CMX system extends the coverage up to pseudorapidity $|\eta| < 1.0$.

III. J/ψ TRIGGER AND SELECTION

Approximately 18% of the J/ψ mesons and 23% of the $\psi(2S)$ mesons produced in $p\overline{p}$ collisions at $\sqrt{s} = 1.8$ TeV come from the decay of B-hadrons [18]. The remainder are either directly produced or come from the decay of directly produced higher mass charmonium states.

In this Section, we describe the data sample and selection cuts common to the lifetime analyses described in this paper. CDF uses a three-level trigger system. The first two levels are hardware triggers, and Level 3 is a software trigger based on a version of the offline reconstruction code optimized for computational speed.

At Level 1, the relevant trigger for the analyses in this paper required the presence of two charged tracks in the central muon chambers (CMU and CMX). At Level 2 there were two different triggers which contributed to the sample.

1. At least one of the muon tracks had to match a track in the CTC found with the Central Fast Track (CFT) processor [19]. The efficiency of finding a track in the 3 GeV/c CFT-bin rose from 50% at 2.6 GeV/c to 94% for $p_T > 3.1$ GeV/c.

2. An additional Level 2 trigger was introduced in Run 1B which required both muon tracks to be matched to a CFT track. In this case the Level 2 CFT trigger threshold was lowered. The 50% efficiency point was at 1.95 GeV/c for the 2 GeV/c CFT-bin reaching the plateau at 2.3 GeV/c.

Finally, the Level 3 software trigger required the presence of two oppositely charged muon candidates with invariant mass between 2.8 and 3.4 GeV/c^2.

Background events in the dimuon sample collected with these triggers are suppressed by applying additional muon selection cuts. First, the separation between the track in the muon chamber and the extrapolated CTC track was calculated in both the transverse and longitudinal planes. In each view, the difference was required to be less than 3.0 standard deviations (σ) from zero, where σ was the sum in quadrature of the multiple Coulomb scattering and measurement errors. Secondly, the energy deposited in the hadronic calorimeter by each muon was required to be greater than 0.5 GeV, the smallest energy expected to be deposited from a minimum ionizing particle. Finally, runs with known hardware problems were removed.

For optimal vertex resolution both tracks were required to be reconstructed in the SVX detector. The invariant mass distribution of pairs of oppositely charged muons is shown in Fig. 2. The invariant mass was calculated after constraining the two muon tracks to come from a common point in space ("vertex constraint") to improve the mass resolution. The resulting width of the J/ψ mass

peak was 16 MeV/c^2. The observed width is dominated by the mass resolution of the tracking detectors since the intrinsic width of the J/ψ is very narrow (87 ± 5 KeV/c^2 [20]). Using a mass window of $\pm$ 50 MeV/c^2 around the J/ψ mass [20] we observe a signal of 243,000$\pm$ 540 J/ψ events over a background of 34,000$\pm$ 130 events. About 19% of the J/ψ candidates were collected during Run 1A.

For the B^+ and B^0 reconstruction, final states having either a J/ψ or $\psi(2S)$ were included. The $\psi(2S)$ candidates were reconstructed from the decay $\psi(2S) \to J/\psi$ $\pi^+\pi^-$ by combining $J/\psi \to \mu^+\mu^-$ events with two additional, oppositely charged tracks. When calculating the invariant mass, each of these two additional tracks was assigned the charged pion mass, and the invariant mass of the two pions was required to be less than 600 MeV/c^2. The two muons from the J/ψ and the two pion tracks were required to come from a common vertex. Events in which the transverse momentum of the four track system was less than 3 GeV/c were rejected. The $\psi(2S)$ candidates were required to be within $\pm$0.02 GeV/c^2 of the world average $\psi(2S)$ mass of 3.686 GeV/c^2 [20]. We found 3577 $\pm$ 97 $\psi(2S)$ candidates passing these requirements. The invariant mass distribution of $\psi(2S)$ candidates is shown in Fig. 3 .

IV. EXCLUSIVE B RECONSTRUCTION

In this Section we will describe the reconstruction of the exclusive B^+, B^0 and B_s^0 decays.

A. Reconstruction of B^+ and B^0 Decays

B^+ mesons were reconstructed in the decay modes J/ψ K^+, J/ψ $K^*(892)^+$, $\psi(2S)$ K^+, and $\psi(2S)$ $K^*(892)^+$. B^0 mesons were reconstructed in the decay modes $J/\psi K_s^0$, $J/\psi K^*(892)^0$, $\psi(2S)$ K_s^0, and $\psi(2S)$ $K^*(892)^0$. The kaons were reconstructed using the decay channels $K_s^0 \to \pi^+\pi^-$, $K^*(892)^0 \to K^+\pi^-$, and $K^*(892)^+ \to K_s^0\pi^+$. Here and throughout this paper π^+ and K^+ refer to a charged track that was assigned the charged pion or kaon mass respectively when combined with other tracks.

Upon the reconstruction of a J/ψ or $\psi(2S)$ candidate, a search for $K_s^0 \to \pi^+\pi^-$ candidates was initiated by considering all pairs of oppositely charged tracks not already assigned to the J/ψ or $\psi(2S)$ candidate. Both tracks were assumed to be charged pions, and the tracks were constrained to come from a common vertex. Since the proper decay length of the K_s^0 is 2.6762 cm [20], it can be tagged by requiring a displaced vertex. The absolute value of the impact parameter with respect to the beam position of both pions was required to be larger than 2σ, where $\sigma^2 = \sigma_m^2 + \sigma_b^2$, σ_m was the measurement uncertainty, and σ_b was the beam spot size (see Section V). The reconstructed K_s^0 was required to have a positive decay length with respect to the J/ψ vertex. The minimum distance between its flight path and the J/ψ vertex was required to be less than 2 mm in the plane transverse to the proton beam. Finally, track pairs with

invariant mass within ± 20 MeV/c^2 of the world average value of 497.672 MeV/c^2 [20] were considered K_s^0 candidates. The invariant mass distribution of K_s^0 candidates is shown in Fig. 4. We found 42,600 candidates in the J/ψ sample. To reconstruct the $K^*(892)^+$, K_s^0 candidates were paired with an additional track assumed to be a charged pion. Tracks from the K_s^0 were both mass and vertex constrained. The K_s^0 π^+ combinations were required to be within ± 80 MeV/c^2 of the average $K^*(892)^+$ mass of 891.59 MeV/c^2 [20]. A relatively wide mass window was necessary because the natural width of the $K^*(892)^+$ is about 50 MeV/c^2 [20].

J/ψ or $\psi(2S)$ candidates were combined with kaon candidates to form B^+ and B^0 candidates. In all cases the invariant mass of the $\mu^+\mu^-$ pair was constrained to the J/ψ mass (mass constraint) $\psi(2S)$ were and the $J/\psi\pi^+\pi^-$ invariant mass was constrained to the $\psi(2S)$ mass. Since the intrinsic widths of the J/ψ and $\psi(2S)$ are significantly less than our experimental resolutions on the invariant masses, a mass constraint improved the resolution on the track parameters. For the J/ψ K^+ and $\psi(2S)$ K^+ modes, the additional track was assigned the charged kaon mass, and the three or five track combination was vertex constrained. For the J/ψ K_s^0, $\psi(2S)$ K_s^0, J/ψ $K^*(892)^+$, and $\psi(2S)$ $K^*(892)^+$ modes, tracks from the K_s^o were both mass and vertex constrained with the requirement that the K_s^0 pointed to the B vertex. For modes with a $K^*(892)^0$, a search was conducted for two oppositely charged tracks to combine with a J/ψ or $\psi(2S)$ candidate. The tracks were assumed to be a $K\pi$ combination and all tracks were vertex constrained. The transverse momenta of the charged kaon and pion were required to be greater than 1.0 and 0.5 GeV/c, respectively. The mass window for $K^*(892)^0$ acceptance was ± 80 MeV/c^2 about the world average value.

Since the B candidate selection process involved searching over all possible tracks, the possibility existed that more than one B candidate per J/ψ or $\psi(2S)$ passed the constraints stated above. Since using overlapping candidates would bias the decay length distribution, only one of these candidates was used in the lifetime calculation. The duplicate removal process occurred in two steps. The first involved filtering candidates whose only difference was the assignment of charged kaon and pion masses to the two-track reconstruction of the $K^*(892)^0$. Since the fit χ^2 probabilities of the $K\pi$ and πK mass assignments were equal, the $K^*(892)^0$ candidate closest to the world average mass value was chosen. The second step was to choose the B candidate having the highest χ^2 probability for fitting N tracks to a common vertex. Real B mesons should usually return a higher quality fitted secondary vertex than background events.

To reduce the statistical uncertainty on the background subtracted signal, we required that the p_T of the B be greater than 6 GeV/c and that the p_T of the K be greater than 1.25 GeV/c.

The distributions of the mass difference between the world average B-mass of 5.279 GeV/c^2 [20] and the reconstructed mass are shown in Fig. 5 and 6 for the charged and neutral B mesons respectively. The upper and lower plots respectively are with and without a 100 μm cut on the proper decay length. Although not used in the lifetime analysis, this requirement illustrates that the background is concentrated at short lifetime values and the enrichment of signal events at large proper decay length values.

B. Reconstruction of the Decay $B_s^0 \to J/\psi\phi$.

The B_s^0 candidates were reconstructed in the decay chain $B_s^0 \to J/\psi\phi$, with $J/\psi \to \mu^+\mu^-$ and $\phi \to K^+K^-$. The method of reconstructing the decay $B_s^0 \to J/\psi\phi$ has been described in detail elsewhere [21]. A brief description is given below.

Once a J/ψ was found, we searched for $\phi \to K^+K^-$ candidates by selecting oppositely charged track pairs that were not muons and reconstructing their invariant mass while assigning each track the mass of a kaon. If this candidate ϕ mass lay within $\pm$ 0.01 GeV/c^2 of the world average ϕ mass of 1.01943 GeV/c^2 [20], then the invariant mass of all four tracks was calculated while constraining them to come from a common vertex and mass constraining the invariant mass of the muon pair to the J/ψ mass.

To improve the signal-to-background ratio, we required that the χ^2 probability of the constrained fit was greater than 1% and that the transverse momenta of the ϕ and B_s^0 were greater than 2.0 GeV/c and 6.0 GeV/c, respectively.

The $J/\psi\phi$ invariant mass spectrum is shown in Fig. 7. A typical uncertainty on the candidate B_s^0 reconstructed invariant mass was 0.01 GeV/c^2. A fit to a Gaussian plus a second order polynomial background is superimposed. A signal of 58$\pm$12 events is observed.

V. THE PRIMARY INTERACTION VERTEX

The lifetimes reported here were determined by measuring the distance between the primary $p\bar{p}$ interaction and the secondary decay vertex in the transverse plane. All the measurements described in this paper used the average beam position as an estimate of the primary vertex. This was calculated offline for each data acquisition run. We chose not to measure the primary vertex event-by-event because the presence of a second b-quark in the event coupled with the low multiplicity in the J/ψ events can lead to a systematic bias in the lifetime. This technique would not improve the statistical uncertainty of the measurements. In the following we describe some of the beam properties.

The distribution of primary vertices in z is shown in Fig. 8. The interaction probability as a function of z was approximately a Gaussian function with a sigma of $\approx$ 30 cm. Near the interaction region, the beams fol-

low a straight line but could have an offset and slope with respect to the z-axis of the tracking detectors. The profile of the beam for a typical data acquisition run is shown in Fig. 9. Plotted is the deviation of reconstructed primary vertices in the transverse plane from the calculated average beam position. To ensure that the spread of the beam and not the resolution of the vertex fit is the dominant contribution to the width of the observed distribution, we used only vertices with high track multiplicity. In addition only tracks with 4 associated clusters in the SVX were used in the vertex fit. The upper two plots show the 2-dimensional distribution of the beam spot for a typical data acquisition run during the 1994-95 running period. The lower two plots show the x and y projections, respectively, with a fit to a Gaussian distribution superimposed. The beam was roughly Gaussian and circular with a σ of 23 μm in x and 22 μm in y for this particular data acquisition run.

These values are averaged over the z-range covered by the two SVX modules and over the run. One expects the σ of the beam to vary weakly in z as [22]

$$\sigma(z) = \sqrt{\epsilon\beta^* \times (1 + ((z - z_0)/\beta^*)^2)}, \qquad (5.1)$$

where ϵ is the transverse emittance, β^* is the amplitude function at the interaction point, and z_0 the z position of the minimum. The variation of the x and y projections of the beam width with z for a typical data acquisition run is shown in Fig. 10. We observed that the width varied by approximately 20% over the length of the SVX. Table I summarizes the results of fitting function (5.1) to the points for one data acquisition run. This set of parameters was typical for the 94-95 running period. The values agree well with the estimates of the Fermilab accelerator division [23].

We also analyzed how the position of the beam varied in time during a data acquisition run. We observed that the beam was very stable in time, rarely moving by more than a few microns during a data acquisition run, resulting in a very small contribution to the variation of the primary vertex position.

VI. THE TRANSVERSE DECAY LENGTH L_{XY}

In this section, we describe the quantities used to measure the lifetime. First, we describe the variables used for the exclusive B-lifetime measurement. Then, we discuss the inclusive case where the momentum of the B is not completely reconstructed and where the J/ψ vertex is used as an estimate for the B-vertex.

The definition of the transverse decay length L_{xy} is shown in Fig. 11. The vector $\vec{X}$ points from the primary vertex $\vec{x}_{prim}$ to the secondary vertex $\vec{x}_B$ in the plane normal to the incoming p beam:

$$\vec{X} = \vec{x}_B - \vec{x}_{prim}. \qquad (6.1)$$

For the primary vertex, we used the calculated beam position. To estimate $\vec{x}_B$, we did a vertex fit to the tracks

emanating from the decay of the B-meson, constraining the tracks to come from a common vertex. The transverse decay length L_{xy} was then defined as the projection of this vector onto the momentum of the B:

$$L_{xy}^B = \frac{\vec{X} \cdot \vec{p_T^B}}{|\vec{p_T^B}|}. \tag{6.2}$$

L_{xy} is a signed variable, that is, it is negative for the configuration where the particle seems to decay before the point where it was produced. For a zero-lifetime sample, one expects a Gaussian distribution peaked at $L_{xy} = 0$. Experimental tests of this expectation are discussed in Section VII E. For the exclusive decays, the proper decay length was

$$\lambda^B = \frac{L_{xy}^B}{(\beta\gamma)_T^B} = L_{xy}^B \cdot \frac{M_B}{p_T^B}, \tag{6.3}$$

where $(\beta\gamma)_T^B$ is the Lorentz factor times $\sin\theta$. For the uncertainty of the transverse decay length, the only relevant contributions came from the uncertainties on the primary and secondary vertex coordinates. Contributions arising from the transverse momentum uncertainties were negligible. For a circular beam spot, the experimental uncertainty in L_{xy} is

$$\begin{aligned}\sigma_{L_{xy}}^2 = & \frac{1}{\left(p_T^B\right)^2} \\ & \times \left[(\sigma_{xv} P_x^B)^2 + 2\sigma_{xyv}^2 P_x^B P_y^B + (\sigma_{yv} P_y^B)^2 \right. \\ & \left. + (\sigma_p P_x^B)^2 + (\sigma_p P_y^B)^2\right]\end{aligned} \tag{6.4}$$

where

σ_{xv}^2, σ_{yv}^2, σ_{xyv}^2 = covariance matrix elements of the secondary vertex fit,
σ_p = sigma of the primary vertex (beam spot),
p_T^B = transverse momentum of B-meson, and
P_x^B, P_y^B = x, y components of B momentum.

In the case of the inclusive lifetime measurement, a fit to the two muons from the J/ψ decay allowed for a good estimate of the B-meson vertex. Since the J/ψ lifetime is much smaller than our detector resolution, its vertex is virtually identical to the B-vertex. From Monte Carlo simulations we estimated that for a J/ψ in our sample the average angle between the J/ψ momentum and the B-hadron momentum was 7.6 degrees and on average the J/ψ carried more than 70% of the B momentum. Therefore, for the inclusive lifetime measurement, the transverse decay length of the B-hadron was approximated by

$$L_{xy}^\psi = \frac{\vec{X} \cdot \vec{p_T^\psi}}{|\vec{p_T^\psi}|}. \tag{6.5}$$

Since we only partially reconstructed the B, we had to correct for the missing momentum in determining the proper decay length. As a first approximation to λ_B, we used the relativistic quantity $(\beta\gamma)_T^\psi$ of the J/ψ, giving

$$\lambda_\psi = \frac{L_{xy}^\psi}{(\beta\gamma)_T^\psi} = L_{xy}^\psi \cdot \frac{M_\psi}{p_T^\psi}. \tag{6.6}$$

The distribution of the calculated uncertainty in L_{xy}^ψ for J/ψ events is shown in Fig. 12. The mean uncertainty on L_{xy}^ψ was 55 μm, which meant that for J/ψ events the contribution from the secondary vertex dominated the uncertainty compared to the primary vertex

($\sigma_p \approx 23\mu m$) contribution. We found that there was no correlation between L_{xy} uncertainty and L_{xy} magnitude. We applied a correction factor $F(p_T^\psi)$ parametrized as a function of the transverse J/ψ momentum p_T^ψ to connect λ_ψ and λ_B,

$$F(p_T^\psi) = \frac{(\beta\gamma)_T^B}{(\beta\gamma)_T^\psi} = \frac{\lambda_\psi}{\lambda_B}. \tag{6.7}$$

The Monte Carlo procedure to obtain the average correction factor is described in Section VII B. With this definition of $\langle F(p_T^\psi)\rangle$, the variable 'pseudo proper decay length' (λ) was defined as

$$\lambda = \frac{\lambda_\psi}{\langle F(p_T^\psi)\rangle} = L_{xy}^\psi \cdot \frac{M_\psi}{p_T^\psi \langle F(p_T^\psi)\rangle}. \tag{6.8}$$

VII. MEASUREMENT OF THE AVERAGE LIFETIME

The average B-hadron lifetime measurement used a subset of the J/ψ data sample described in Section III. Only the Run 1B data sample and only J/ψ candidates selected by the level 2 trigger requiring both muons to be matched to a CFT track were used, leaving 167,000 candidates. As we show later, the precision of this measurement is limited by systematics, so including the additional 31% of data would not improve the result.

The steps in measuring the B lifetime from the inclusive J/ψ sample were:

- Measure the 2-dimensional decay length L_{xy} for the J/ψ meson sample.
- Correct the measured L_{xy} of the J/ψ mesons for the difference between the $(\beta\gamma)_T^\psi$ of the J/ψ mesons and the $(\beta\gamma)_T^B$ of the B hadron. The distribution of this corrected decay distance, which closely approximates the proper decay length distribution of the B mesons, was called the pseudo proper decay length (λ) distribution.
- Measure the λ distribution of the background under the J/ψ by studying the $\mu^+\mu^-$ mass sidebands of the J/ψ.
- Fit the λ distribution to the sum of background, direct (zero-lifetime) and B decay (non-zero lifetime) contributions and extract the lifetime.

We describe each of these steps in more detail below.

A. Track and Vertex Selection

More than 80% of the J/ψ sample consisted of prompt J/ψ mesons. When extracting the lifetime we assumed Gaussian resolution. Any non-Gaussian component that we have not taken into account in the fit could bias the lifetime measurement. To make sure that the vertex was well measured, to reduce non-Gaussian tails and to have good understanding of the σ of the vertex fit we applied strict track and vertex quality cuts. In addition to the cuts described in Section III, the following cuts were applied:

1. Both muons were required to have associated clusters in all four layers of the SVX.

2. For the SVX track fit (4 degrees of freedom), we required $\chi^2/\mathrm{DoF} < 5$.

3. For the calculated uncertainty on the decay length we required: $\sigma_{L_{xy}} < 150\mu m$.

4. For the vertex fit we required $\chi^2_{Vertex} < 12$.

In addition, we required $p_T^\psi > 4$ GeV/c to reduce the overall uncertainty of the measurement. This reduced the statistics but also reduced the systematic uncertainties which dominated the precision of this measurement.

The reduction in systematic uncertainty came from several sources. First, the average correction factor $\langle F(p_T^\psi)\rangle$ varies only weakly for $p_T^\psi > 4$ GeV/c (see Sec. VII B). Second, this cut is away from the turn-on of the trigger. Monte Carlo studies done by varying the parameters of the production and decay kinematics showed that the differences between the various models were important at low p_T but were less significant at higher p_T. In addition the transverse momentum of J/ψ mesons from B-decays was stiffer than that of prompt J/ψ's so this cut enriched the fraction of J/ψ mesons from B-hadron decays.

We have 67,800 pairs of oppositely charged muons in the signal region and 7,900 pairs in the combined two sideband regions after all cuts.

B. Monte Carlo Procedure to Determine $\langle F(p_T^\psi)\rangle$

Monte Carlo events were used to determine the average correction factor $\langle F(p_T^\psi)\rangle$ and to study the systematic variations due to production and decay kinematics.

The b-quarks were generated with the p_T-spectrum from the next to leading order QCD calculation of Nason, Dawson and Ellis (NDE) [24]. As a comparison and for systematic studies, we also generated events according to a power law distribution defined as

$$\frac{d\sigma}{dp_T^2} = \frac{A}{(p_T^2 + m_b^2)^n}, \tag{7.1}$$

where m_b and n are constants. The choice of m_b=4.75 and n=2.0 gave the best agreement with the data.

The hadronization of the b-quarks was modeled using the Peterson fragmentation function [25] with $\epsilon_b = 0.006$ as the value of the fragmentation parameter. We used the following fragmentation fractions for the hadronization into different b-flavored hadrons: $f_u : f_d : f_s : f_{\Lambda_b} = 0.375 : 0.375 : 0.15 : 0.10$ which is consistent with our measurement [26]:

$$\begin{aligned} f_u &= 0.39 \pm 0.04 \pm 0.04, \\ f_d &= 0.38 \pm 0.04 \pm 0.04, \\ f_s &= 0.13 \pm 0.03 \pm 0.01, \\ f_{\Lambda_b} &= 0.096 \pm 0.017. \end{aligned}$$

The decay of the B-hadrons was then modeled using the QQ Monte Carlo developed by the CLEO collaboration [27,28]. The resulting long-lived particles served as input to a full simulation of the CDF detector and triggers. The trigger efficiencies as a function of p_T were well understood and were discussed in Section III.

For each step of the simulation process, the relevant model parameters were varied to estimate the systematic uncertainties in modeling the production and decay.

Figure 13 compares the p_T-spectrum derived from the data along with the Monte Carlo predictions. To ensure that this J/ψ p_T-spectrum represented J/ψ mesons from b-decay, the distribution was background subtracted, and the proper decay length was required to be larger than 200 μm. The number of Monte Carlo events were normalized to the number of data events with $P_T^\psi > 4.0$ GeV/c. Compared to the data, the power law Monte Carlo produced a spectrum which was softer, whereas that from NDE was harder.

The correction factor $\langle F(p_T^\psi)\rangle$ (see Fig. 14) was obtained by averaging $(\beta\gamma)_T^B/(\beta\gamma)_T^\psi$ for different bins in p_T^ψ. We observed that for $p_T^\psi > 5.0$ GeV/c the correction factor was a constant. The superimposed fit has the following functional form:

$$F(p_T^\psi) = B \cdot exp(C \cdot p_T^\psi) + D$$

where B, C, and D are constants.

C. Fitting Technique

The fitting techniques, as well as the background and signal parametrizations, are discussed in this section. The fit to the lifetime distribution was done in two steps. First, we fit the λ distribution of the J/ψ sidebands to get the shape of the background. The background under the signal was assumed to have the same shape as in the sidebands. Then the events in the signal mass region were fit holding all parameters from the sideband fit except the number of events constant. The number of background events was constrained within Poisson fluctuations to the number of sideband events N_{SB} divided by a factor of 2, since the sideband invariant mass windows were twice as large as that of the signal region and the distribution was assumed to be flat.

The shape of the background was obtained by parametrizing the λ distribution of the sidebands $2.9 < M_\psi < 3.0$ GeV/c^2 and $3.2 < M_\psi < 3.3$ GeV/c^2 as the sum of three terms: a central Gaussian, a left side exponential and a right side exponential. The two exponentials account for any non-Gaussian tails. We expect some enhancement of events with positive λ due to the presence of sequential semileptonic B decays in the dimuon sample. Therefore the fractions and slopes of the left and right side exponential could be different. For each sideband event with the measured pseudo proper decay length λ_j and its calculated uncertainty σ_j, the background distribution function was defined as:

$$g_{bkg}(\lambda_j,\sigma_j) = \begin{cases} \text{for } \lambda_j \geq 0: \\ (1-f^+-f^-)\frac{e^{-\lambda_j^2/2(s\sigma_j)^2}}{\sqrt{2\pi}s\sigma_j} + \frac{f^+}{\lambda^+}e^{-\lambda_j/\lambda^+} \\ \text{and for } \lambda_j < 0: \\ (1-f^+-f^-)\frac{e^{-\lambda_j^2/2(s\sigma_j)^2}}{\sqrt{2\pi}s\sigma_j} + \frac{f^-}{\lambda^-}e^{\lambda_j/\lambda^-} \end{cases} \quad (7.2)$$

where

s = the error scale factor,
f^+ = the fraction of the right side exponential,
λ^+ = the slope of the right side exponential,
f^- = the fraction of the left side exponential,
λ^- = the slope of the left side exponential.

The pseudo λ distribution for the signal region, defined as $\pm$ 50 MeV/c^2 around the J/ψ mass, consisted of three components: a Gaussian distribution for the prompt J/ψ mesons, the background distribution $g_{bkg}(\lambda_j, \sigma_j)$ and an exponential convoluted with a Gaussian resolution function $F_s(\lambda_j, \sigma_j) = G * E$ to describe the J/ψ mesons from b-decay. For each measured pseudo proper decay length λ_j and its calculated uncertainty σ_j, the signal distribution function was defined as

$$f(\lambda_j, \sigma_j) = f_{bkg} g_{bkg}(\lambda_j, \sigma_j) + (1 - f_{bkg}) \times \left[\frac{1 - f_B}{\sqrt{2\pi} s \sigma_j} \cdot e^{-\lambda_j^2 / 2(s\sigma_j)^2} + f_B \cdot F_s(\lambda_j, \sigma_j) \right], \quad (7.3)$$

where

λ_B was the mean proper B decay length,
f_B was the fraction of J/ψ from B decay,
s was the error scale factor, and
f_{bkg} was the background fraction.

The convolution was defined as

$$F_s(\lambda_j, \sigma_j) = \frac{1}{\sqrt{2\pi} s \sigma_j \lambda_B} \int_0^\infty e^{\frac{-(ct - \lambda_j)^2}{2(s\sigma_j)^2}} e^{\frac{-ct}{\lambda_B}} d(ct). \quad (7.4)$$

We used an unbinned maximum likelihood fit to extract the lifetime from the data. A binned likelihood fit provided a check of our method and was used for systematic studies. The unbinned maximum likelihood fit used $f(\lambda_j, \sigma_j)$ as the probability distribution function. The likelihood function was defined as:

$$L = \mathcal{P}(0.5 \times N_{SB}) \times \prod_1^N f(\lambda_j, \sigma_j; f_B, \lambda_B, s) \quad (7.5)$$

where N was the total number of J/ψ candidates, λ_j was the pseudo proper decay length and σ_j was the calculated error for J/ψ_j. The term $\mathcal{P}(0.5 \times N_{SB})$ represents the Poisson term constraining the number of background events within Poisson fluctuations to half the number of sideband events. The corresponding log-likelihood function $\mathcal{L} = -2ln(L)$ was minimized with respect to the parameters f_B, λ_B and s.

The modelling of the λ distribution is incomplete. An additional smearing from the $\beta\gamma$-correction, increasing linearly with pseudo cτ, was not modeled by our fitting function. Rather than modifying the fitting function we correct for the introduced bias. Monte Carlo studies showed that the use of the pseudo $c\tau$ variable λ introduced a bias of 0.5% towards longer lifetime.

To check if the bias depended on the lifetime value, we examined Monte Carlo samples generated with proper decay lengths between 400 and 500 μm and found no dependence. When quoting the final lifetime result, we correct for this bias.

D. Results of Fit to the Data

Table II summarizes the results of the background fits to the sidebands and the signal region. The background clearly had non-Gaussian tails. In addition, the distribution was clearly asymmetric, with a larger tail at positive

lifetime. The presence of the nonzero lifetime component in the background sample was not surprising. The asymmetry is due to sequential semileptonic B decays in the dimuon sample. No such enhancement was observed when using a sample of 'fake' J/ψ's obtained from QCD jet events by selecting oppositely charged track pairs in the same kinematic range as the 'true' dimuon data.

The λ distribution for the signal region with the fit superimposed is shown in Fig. 15. The dark shaded area shows the contribution from background where the shape has been derived from the sidebands and the magnitude has been derived by normalizing the number of sideband events within poisson fluctuations to the same range in invariant mass as used for the signal. The light shaded region shows the contribution due to adding the exponential distribution from b-decay convoluted with a Gaussian resolution function to the background. The remaining unshaded region shows the contribution from prompt J/ψ mesons.

E. Error Scale and Resolution Function.

The error in the proper decay length resolution was an important component of the shape of the probability function used for the unbinned fit. A zero-lifetime sample should be a Gaussian distribution peaked at $L_{xy} = 0$. If the L_{xy} distribution was normalized by its error, $L_{xy}/\sigma_{L_{xy}}$, the resulting Gaussian distribution should have a sigma of unity. Here we present some experimental checks of this assumption.

A sample of track pairs selected from QCD jet events showed that the proper decay length resolution function for tracks coming from the primary vertex was symmetric and centered at zero.

Using $\Upsilon(1S) \to \mu^+\mu^-$ events provided us with a sample of prompt decays of a heavy particle into two muons. The invariant mass spectrum of oppositely charged muon pairs in the $\Upsilon(1S)$ mass region is shown in Fig. 16(A). Figure 16(B) shows the L_{xy} distribution of $\Upsilon(1S)$ mesons after sideband subtraction. The shape is Gaussian, the mean of the distribution is consistent with zero, and the resolution is 43 μm. The $L_{xy}/\sigma_{L_{xy}}$ distribution after sideband subtraction is shown in Fig. 16(C) . A fit of a Gaussian function to the distribution yields a sigma of 1.13 indicating that the calculated error $\sigma_{L_{xy}}$ was underestimated by 13% in average. Finally the $L_{xy}/\sigma_{L_{xy}}$ distribution for the J/ψ sample is shown in Fig. 16(D). A fit to the prompt part of the distribution indicated that the error was underestimated by 13%, which is in good agreement with the scale factor 1.15 ± 0.05 obtained from the lifetime fit.

F. Systematic Errors

In this Section, we describe the sources of systematic uncertainties, which apply to the inclusive lifetime measurement and estimate their magnitude. Two sources of systematic uncertainties apply to all measurements de-

scribed in this paper. These are the alignment of the silicon detector and any bias arising from a possible impact parameter dependence of the CFT trigger. We describe these two systematic uncertainties first and then describe the systematics specific to the inclusive measurement.

1. Alignment of the Silicon Vertex Detector

Details of the SVX alignment procedure and checks of the alignment can be found in reference [16]. When tracks were used to align the detector, the radius of the fourth SVX layer was kept constant while the radial positions of the three inner layers were allowed to float. Significant radial shifts of the order of 80 μm between the optical survey alignment constants and the track based alignment constants were observed. The sign of the shift reversed depending on whether the strips were facing toward (layer 0) or away from the beampipe (layers 1 and 2).

To estimate the uncertainty due to the length scale of the SVX, we compared the lifetime result obtained using alignment constants derived from the optical survey with the result using the track based alignment having the radial shifts. We used a binned fit for this comparison since this fit was not as sensitive to the error scale as the unbinned fit. In the data, we observed a lifetime which is 0.3% smaller when using the track based alignment. This was consistent with the result of a high statistics Monte Carlo study where we compared the result of the lifetime fit before and after the radial positions of the inner silicon layer had been varied. Therefore, we assigned a 0.3% systematic uncertainty to the SVX length scale.

2. Impact Parameter Dependence of the Trigger

The track impact parameter was defined as the closest approach of the track helix to the beam axis measured in the plane perpendicular to the beam. Any variation of the CFT trigger efficiency with the magnitude of the track impact parameter would bias the lifetime distribution. Although the CFT algorithm is based upon prompt tracks, we did not expect a lifetime bias from the CFT since the impact parameter resolution of this device was > 50 times that of the SVX and 3 times the average displacement of secondary tracks from B decay. To check for any possible bias, a sample of J/ψ events was selected by a Level 2 trigger which required only one of the two muons to be reconstructed by the trigger track processor. The second muon then could be used to study the efficiency of the CFT. We observed that the trigger efficiency did not vary with the impact parameter resulting in a negligible effect on the lifetime distribution.

3. Production and Decay Kinematics

Since the $\langle F(p_T^{\psi})\rangle$ was used in the calculation of the pseudo proper decay length variable, any variation in $\langle F(p_T^{\psi})\rangle$, such as from variation of the production and decay kinematics of the event, would affect the inclusive

b-lifetime. In order to understand systematics due to the model dependence, the following studies were done:

- Compare the NDE b-quark p_T spectrum to a power law spectrum.
- Vary the Peterson fragmentation parameter $\epsilon = 0.006$ by ± 0.002 where the value and its uncertainty were taken from [29].
- Vary the value of the B_s^0 meson cross section by $\pm 1\sigma$ [26].
- Vary the level 2 trigger parametrization by $\pm 1\sigma$.
- Vary the polarization of the J/ψ by the allowed range from current CDF results [30].
- Vary the percentage of Λ_b from 5 to 15% of the total b particles produced. The nominal value was 10%.

B_c production was assumed to be very small [31] and was not considered in the systematics. Table III summarizes the $\langle \tau_b \rangle$ uncertainties due to each of these variables.

4. Background Parametrization

We estimated the systematics due to the background parametrization by

- varying by one sigma all the parameters of the background fit coherently in terms of their effect on the lifetime,
- trying different parametrizations of the background distribution function,
- using the smoothed histogram for the background function, and
- letting the background fraction f_{bkg} float in the fit.

After all these checks, we assigned a systematic uncertainty of $\pm$ 0.4% to the background parametrization.

5. Fitting Procedure Bias

As described in Section VII C, the incomplete modelling of the λ distribution introduced a bias of 0.5% towards a longer lifetime that we correct for. We assign the total difference of 0.5% as systematic error.

6. Summary of Systematic Errors

The systematic uncertainties and their quadratic sum are summarized in Table IV. The dominant contribution arises from modeling the production and decay kinematics.

G. Final Average Lifetime Result

The measured B lifetime, which is the average over all B-hadrons produced in $p\overline{p}$ collisions at $\sqrt{s} = 1.8$ TeV weighted by their production cross sections, branching ratios to J/ψ, and detection efficiencies, is

$$\langle \tau_b \rangle = 1.533 \pm 0.015 \text{ (stat)} \, ^{+0.035}_{-0.031} \text{ (syst) ps}$$

VIII. B^0 AND B^+ LIFETIMES

In this Section we discuss how we determined the lifetime of the B^+ and B^0. The reconstruction of the B^+ and B^0 has been described in Sec. IV. We also discuss the systematic errors on these measurements.

A. Fitting Technique

Since there were fewer B^0 and B^+ events, the fitting was done slightly differently from the inclusive lifetime case. Here we performed a simultaneous, unbinned log-likelihood fit on both the signal and sideband events. The sideband events plus the background events under the peak were used to determine the shape of the proper decay length distribution of the background in the signal region. Thus, more statistics were used for the determination of the background than in the two stage fit.

1. Background Parametrization

We used two sideband regions where the upper and lower sideband windows were each 60 MeV/c^2 wide and started at $\pm$60 MeV/c^2 from the world average value B-mass of 5.279 GeV/c^2 [20]. The width of the sideband mass windows and the two 30 MeV/c^2 wide separations between the signal and sideband regions significantly reduced the probability that real B mesons where one pion hasn't been reconstructed appear in the sidebands. The background events in the peak region were assumed to have the same proper decay length distribution as events in the sideband regions. The λ distribution of background and sideband events was parametrized as a Gaussian for the zero-lifetime events, two exponentials for the positive lifetime background, and an exponential for the negative lifetime background. Two exponentials were needed for positive lifetimes to accurately fit the data. This gave the background distribution as

$$g_{bkg}(\lambda_j,\sigma_j) = \begin{cases} \text{for } \lambda_j \geq 0: \\ \frac{1-f_1^- -f_1^+ -f_2}{\sigma_j\sqrt{2\pi}} \cdot e^{-\lambda_j^2/2\sigma_j^2} + \frac{f_1^+}{\lambda_1} e^{-\lambda_j/\lambda_1} \\ +\frac{f_2}{\lambda_2} e^{-\lambda_j/\lambda_2} \\ \\ \text{and for } \lambda_j < 0: \\ \frac{1-f_1^- -f_1^+ -f_2}{\sigma_j\sqrt{2\pi}} \cdot e^{-\lambda_j^2/2\sigma_j^2} + \frac{f_1^-}{\lambda_1} e^{\lambda_j/\lambda_1} \end{cases} \tag{8.1}$$

where λ_j is the proper decay length for event j, σ_j is the calculated error on λ_j. The fitting parameters are summarized in the next Section.

2. Signal Distribution and Likelihood Function

The peak region, defined as $\pm$30 MeV/c^2 about the world average B mass, contained both signal and background events. For true B meson candidates in this region, the proper decay length distribution was parametrized as the convolution of an exponential function with a Gaussian resolution function $F_s(\lambda_j,\sigma_j) = G * E$, as defined in equation 7.4 in Section VII C. The fitting function was

$$h_{fit}(\lambda_j,\sigma_j) = \begin{cases} \text{for the signal region:} \\ (1-\alpha)\cdot g_{bkg}(\lambda_j,\sigma_j) \\ +\alpha \cdot F_s(\lambda_j,\sigma_j) \\ \\ \text{for the sideband regions:} \\ g_{bkg}(\lambda_j,\sigma_j). \end{cases} \tag{8.2}$$

Here α was the fraction of signal and (1 - α) the fraction of background events in the signal region. The number of background events was constrained within Poisson fluctuations to the number of sideband events divided by a factor of 2, since the sideband invariant mass windows were twice as large as that of the signal region and the distribution was assumed to be flat. The eight fit parameters were

λ_B	: mean proper decay length of the signal,
α	: fraction of signal in the peak region,
events	: number of fitted signal events,
f_1^-	: fraction of negative tail of the background,
f_1^+	: fraction of positive tail of the background,
f_2	: fraction of additional positive tail of the background,
λ_1	: slope of negative and positive tails, and
λ_2	: slope of additional positive tail.

The likelihood function was

$$L = \prod_1^N h_{fit}(\lambda_j, \sigma_j) \tag{8.3}$$

The log-likelihood function to be minimized was $\mathcal{L} = -2ln(L)$.

B. Results of Fit to the Data

The fitted values are listed in Table V for the charged and neutral B mesons. The proper decay length distributions with the fits superimposed are shown in Figures 17 and 18.

As an independent cross check, we extracted the number of B candidates by fitting a Gaussian plus a linear background to the invariant mass distributions (see Fig. 5 and 6). Within the statistical errors, these numbers agree well with the number of events listed in Table V.

C. Systematic Errors

There were four significant contributions to the systematic error: (1) a possible bias due to the fitting technique, (2) the radial length scale of the SVX, (3) non-Gaussian tails of the resolution function, and (4) uncertainty in the event-by-event proper length error.

1. Fitting Procedure Bias

To determine any bias from the fitting procedure we generated 1000 Monte Carlo proper decay length distributions to mimic the data for B^+ and B^0 candidates. After applying the simultaneous fit, the minimized value for $\mathcal{L}$ was calculated. The bias due to the fitting procedure was defined as the mean difference between the fitted lifetime value and the input to the Monte Carlo. We found a bias 1 μm for the B^+ and 2 μm for the B^0 and assigned the total difference as a systematic error.

2. Length Scale of the SVX

The uncertainty of the length scale is a systematic error inherent to the data sample. This uncertainty was discussed in Section VII F 1 covering the systematic uncertainties of the inclusive B lifetime measurement.

3. Non-Gaussian Tails of the Resolution Function

To estimate the lifetime bias from non-Gaussian tails of the resolution function, we added exponential tails to the

Gaussian. The new resolution function was then defined as

$$\mathcal{R}(\lambda) = \begin{cases} \frac{1-\beta}{\lambda_{tail}} \cdot e^{-\lambda/\lambda_{tail}} + \beta \cdot G & \text{for } \lambda \geq 0 \\ \frac{1-\beta}{\lambda_{tail}} \cdot e^{\lambda/\lambda_{tail}} + \beta \cdot G & \text{for } \lambda < 0 \end{cases} \quad (8.4)$$

Substituting $\mathcal{R} * E$ for $G * E$ in Equation 8.2 adds two new parameters, λ_{tail} and β, to the fit. We assigned half the difference between the lifetimes obtained with the two parametrizations as a systematic error. This added 1.2 and 1.1% to the systematic uncertainties for B^+ and B^0, respectively. This is the dominant systematic uncertainty.

4. Error Scale

To evaluate the uncertainty in the lifetimes arising from any uncertainty of the error scale, we introduced a common scale factor for the measurement errors as an additional fit parameter as we did for the measurement of the inclusive lifetime. We assigned half the difference obtained with or without the scale factor to this uncertainty.

5. Summary of Systematic Errors

The systematic errors are listed in Table VI. For the B^+ and B^0 the sum in quadrature adds up to 1.3 % and 1.2 % respectively. The uncertainty due to the length scale are completely correlated in the B^+ and B^0 lifetime measurements.

D. Final Result for $\tau(B^+)$, $\tau(B^0)$ and the Ratio $\tau(B^+)/\tau(B^0)$

The results of this analysis are summarized here:

$$\tau(B^+) = 1.68 \pm 0.07\,(\text{stat}) \pm 0.02\,(\text{syst})\ \text{ps}$$

$$\tau(B^0) = 1.58 \pm 0.09\,(\text{stat}) \pm 0.02\,(\text{syst})\ \text{ps}$$

$$\tau(B^+)/\tau(B^0) = 1.06 \pm 0.07\,(\text{stat}) \pm 0.02\,(\text{syst}).$$

When calculating the uncertainty on the lifetime ratio, we remove the correlated systematic uncertainties as indicated in the previous Section. Although the measured B^+ lifetime is slightly larger than the measured B^0 lifetime, as expected from some theoretical models, the current level of statistics is insufficient to make a definitive statement.

IX. THE B_S^0 LIFETIME

The B_s^0 lifetime was determined by measuring a positive proper decay length exponential as in the previous cases. Due to a more limited number of B_s^0 candidates, a simultaneous log-likelihood fit was done to the invariant mass and lifetime distributions.

A. Fitting Technique

1. The $c\tau$ Distribution

The signal region was defined as the invariant mass range: 5.1 to 5.7 GeV/c^2. The mass range was relatively wide so that the background shape was better determined. The background proper decay length distribution

$g_{bkg}(\lambda_j, \sigma_j)$ was parametrized in the same way as for the inclusive lifetime measurement (see equation 7.2 in Section VII C) as the sum of three terms: a central Gaussian, a left side exponential, and a right side exponential.

For true B_s^0 meson candidates in the signal region, the proper decay length distribution was parametrized as the convolution of an exponential function with a Gaussian resolution function, $F_s(\lambda_j, \sigma_j) = G * E$, as defined in equation 7.4 in Section VII C.

2. The Invariant Mass Distribution

The invariant mass distribution $g(m_j)$ for the background was parametrized as a second order polynomial

$$g(m_j) = p_0 + p_1 m_j + p_2 (m_j - M_{B_s^0})^2, \tag{9.1}$$

where m_j is the $J/\psi\phi$ invariant mass and $M_{B_s^0}$ is the B_s^0 meson mass. There was one equation of constraint due to the normalization condition

$$\int_{m_1}^{m_2} g(m_j) dm_j = 1, \tag{9.2}$$

where m_1 (5.1 GeV/c^2) to m_2 (5.7 GeV/c^2) was the mass range of B_s^0 candidates used in the fit. Therefore, the fit was done for p_1 and p_2 with p_0 expressed in terms of these two.

The invariant mass distribution of the signal was parametrized as a Gaussian distribution with mean M_{B_s},

$$G_m(m_j, \sigma_{m_j}) = \frac{1}{\sqrt{2\pi}\sigma_{m_j}} e^{-\frac{(m_j - M_{B_s^0})^2}{2\sigma_{m_j}^2}}. \tag{9.3}$$

The calculated invariant mass of event j was m_j, and the error of the calculated invariant mass was σ_{m_j}.

3. Bivariate Probability Distribution and Likelihood Function

The normalized bivariate probability density function for a simultaneous mass and lifetime fit is

$$f(\lambda_j, m_j, \sigma_j, \sigma_{m_j}) = (1 - f_s) g(m_j) g_{bkg}(\lambda_j, \sigma_j) + f_s G_m(m_j, \sigma_{m_j}) F_s(\lambda_j, \sigma_j). \tag{9.4}$$

where f_s was the fraction of signal events. The likelihood function was

$$L = \prod_1^N f(\lambda_j, m_j, \sigma_j, \sigma_{m_j}). \tag{9.5}$$

The log-likelihood function to be minimized was $\mathcal{L} = -2ln(L)$. The ten fit parameters were

$\lambda_{B_s^0}$	: B_s^0 lifetime,
f_s	: fraction of signal events,
f^+	: fraction of right side exponential,
λ^+	: slope of right side exponential,
f^-	: fraction of left side exponential,
λ^-	: slope of left side exponential,
s	: error scale factor,
M_{B_s}	: B_s^0 mass,
p_1	: first parameter of second order polynomial,
p_2	: second parameter of second order polynomial.

B. Results of Fit to the Data

The result of performing the 10 parameter fit to the data is summarized in Table VII.

The fit signal corresponded to 58 ± 9 events, obtained by multiplying f_s by the total number of events in the sample (804). This, however, yielded an error that did not correctly account for fluctuations in the number of events. To determine the error correctly, the fit of the mass spectrum was done while allowing the number of events to float. This gave 58 ± 12 events.

A plot of the proper-decay length spectrum is given in Fig. 19 for candidates within ± 0.05 GeV/c^2 of the fitted B_s^0 mass. The invariant mass distribution was shown in Fig. 7. As a cross check, we applied the fitting method used to determine the B^0 and B^+ lifetimes to the B_s^0 case. We found $\lambda_{B_s^0}$=383 ± 63 μm for the mean B_s^0 decay length, which is in good agreement with the value of 402 ± 61 μm obtained with the bivariate fitting method.

C. Systematic Errors

We considered the following three systematic uncertainties:

1. The uncertainty due to a possible length scale uncertainty of the SVX has been described in Section VII F 1.

2. An uncertainty in the parametrization of the background. discussed in detail below.

3. An uncertainty due to a possible bias in the fitting procedure,

Point 2 and 3 are discussed in detail below.

1. Background Parametrization

Shifts in the B_s^0 fitted lifetime due to changes in the shape fitted to the background proper decay length distribution were studied for several effects. The resulting shifts were combined in quadrature to assign a final uncertainty. The effects which were studied and the corresponding shifts are listed here.

1. A flat contribution was added to the long-lived background and fitted for the fraction of events distributed flat in λ. This fraction converged to 0.0 with an error of ± 0.1. Then the flat-background fraction was fixed to 0.1, and the lifetime distribution was fit again. The observed shift in lifetime was 1%.

2. The positive long-lived background was modeled as an exponential decay function. This was replaced with an exponential convoluted with a Gaussian resolution function, and the lifetime distribution was fit again. The corresponding shift in lifetime was 0.25%.

3. The mass distribution was fit with either a second order polynomial or a flat distribution. The difference in lifetime from the two methods was 3.4%. This is the largest source of uncertainty for the background parametrization category.

Adding these in quadrature resulted in a total uncertainty of 3.5% from possible alternative background parametrizations.

2. Fitting Procedure Bias

A possible bias in the fitting procedure was studied by generating several thousand mass and lifetime distribu-

tions modeled after the data. The mean of the lifetimes measured was consistent with the generated value with an uncertainty of 0.5%, which we assign as the systematic error.

3. Summary of Systematic Errors

The total systematic uncertainty from all these effects was 3.5%, as summarized in Table VIII.

D. Final Result for $\tau(B_s^0)$

In conclusion, the B_s^0 lifetime has been measured in a hadronic collider in an exclusive decay mode. The result is

$$\tau(B_s^0) = 1.34^{+0.23}_{-0.19}\,(\text{stat}) \pm 0.05\,(\text{syst})\text{ps}.$$

X. SUMMARY AND CONCLUSIONS

All CDF lifetime measurements which include a J/ψ in the final state are summarized below:

$$\begin{aligned}
\langle\tau_b\rangle &= 1.533 \pm 0.015\,(\text{stat})\ ^{+0.035}_{-0.031}\,(\text{syst})\text{ ps}\\
\tau(B^+) &= 1.68 \pm 0.07\,(\text{stat}) \pm 0.02\,(\text{syst})\text{ ps}\\
\tau(B^0) &= 1.58 \pm 0.09\,(\text{stat}) \pm 0.02\,(\text{syst})\text{ ps}\\
\tau(B^+)/\tau(B^0) &= 1.06 \pm 0.07\,(\text{stat}) \pm 0.02\,(\text{syst})\\
\tau(B_s^0) &= 1.34^{+0.23}_{-0.19}\,(\text{stat}) \pm 0.05\,(\text{syst})\text{ps}
\end{aligned}$$

The results are consistent with other B lifetime measurements [10–12]. The current world best average lifetimes can be found in [13]. The average lifetime of the B-hadron species is expected to be smaller than the B^+ or B^0 lifetimes due to contributions from B-baryon decays, which are measured to have shorter lifetimes [5]. The data is consistent with the theoretical prediction that the charged B-meson lifetime $\tau(B^+)$ and the neutral B-meson $\tau(B^o)$ are nearly equal.

Acknowledgments: We thank the Fermilab staff and the technical staffs of the participating institutions for their vital contributions. This work was supported by the U.S. Department of Energy and National Science Foundation; the Italian Istituto Nazionale di Fisica Nucleare; the Ministry of Education, Science and Culture of Japan; the Natural Sciences and Engineering Research Council of Canada; the National Science Council of the Republic of China; the A. P. Sloan Foundation; and the Alexander von Humboldt-Stiftung.

[1] References to a specific charge state imply the charge-conjugate state as well.
[2] I. I. Bigi *et al.*, in "B Decays", edited by S. Stone (World Scientific, New York,1994), p.132; M. B. Voloshin and M. A. Shifman, Sov. Phys. JETP **64**, 698 (1986); I. I. Bigi *et al.*, CERN-Th.7132/94 (1994); I. I. Bigi, UND-HEP-95-BIG02 (1995).
[3] M. Neubert, Int. J. Mod. Phys. A **11**, 4173 (1996).
[4] I. I. Bigi, N.G. Uraltsev, Phys. Lett. B **280**, 120, (1992).
[5] ALEPH Collaboration, D. Buskulic *et al.*, Phys. Lett. B **384** 449 (1996); CDF Collaboration, F. Abe *et al.*, Phys. Rev. Lett. **77** 1439 (1996); DELPHI Collaboration, P.Abreu *et al.*, Zeit. Phys. C **71** 199 (1996); DELPHI Collaboration, P.Abreu *et al.*, Zeit. Phys. C **68** 375 (1995); DELPHI Collaboration, P.Abreu *et al.*, Zeit. Phys. C **68** 541 (1995); OPAL Collaboration, R. Akers *et al.*, Zeit. Phys. C **69** 195 (1996); OPAL Collaboration, R. Akers *et al.*, Phys. Lett. B **353** 402 (1995).
[6] CDF Collaboration, F. Abe *et al.*, Phys. Rev. Lett. **71**, 3421 (1993).
[7] CDF Collaboration, F. Abe *et al.*, Phys. Rev. Lett. **72**, 3456 (1994); CDF Collaboration, F. Abe *et al.*, Phys. Rev. Lett. **76**, 4462 (1996).

[8] CDF Collaboration, F. Abe *et al.*, Phys. Rev. Lett. **74**, 1945 (1995).
[9] CDF Collaboration, F. Abe *et al.*, Phys. Rev. Lett. **77**, 1945 (1996).
[10] ALEPH Collaboration, D. Buskulic *et al.*, Phys. Lett. B **369** (1996) 151; L3 Collaboration, O. Adriani *et al.*, Phys. Lett. B **317** (1993) 474; OPAL Collaboration, P. D. Acton *et al.*, Zeit. Phys. C **60** (1993) 217; ALEPH Collaboration, D. Buskulic *et al.*, Phys. Lett. B **314** (1993) 459; DELPHI Collaboration, P. Abreu *et al.*, Zeit. Phys. C **63** (1994) 3; DELPHI Collaboration, P. Abreu *et al.*, Phys. Lett. B **377** (1996) 195; OPAL Collaboration, P. D. Acton *et al.*, CERN–PPE/96–137, Submitted to Zeit. Phys. **C**; SLD Collaboration, K. Abe *et al.*, Phys. Rev. Lett. **75** (1995) 3624.
[11] SLD Collaboration, K. Abe *et al.*, Phys. Rev. Lett. **79**, 590 (1997); ALEPH Collaboration, D. Buskulic *et al.*, Z. Phys. C **71**, 31 (1996); DELPHI Collaboration, P.Abreu *et al.*, Z. Phys. C **68**, 13 (1995); DELPHI Collaboration, P.Abreu *et al.*, Report No. CERN-PPE/96-139,1996; OPAL Collaboration, R. Akers *et al.*, Z. Phys. C **67**, 379 (1995); DELPHI Collaboration, W. Adam *et al.*, Z. Phys. C **68**, 363 (1995).
[12] ALEPH Collaboration, D. Buskulic *et al.*, Phys. Lett. B **377** 205 (1996); ALEPH Collaboration, D. Buskulic *et al.*, Zeit. Phys, C **69** 585 (1996); DELPHI Collaboration, P.Abreu *et al.*, Zeit. Phys. C **71** 11 (1996); OPAL Collaboration, R. Akers *et al.*, Phys. Lett. B **350** 273 (1995).
[13] Particle Data Group, 1997 WWW Review of Particle Physics, http://pdg.lbl.gov/1997/mxxx.html; LEP B lifetimes working group, http://wwwcn.cern.ch/ claires/lepblife.html; For a recent overview see, e. g., J. D. Richman, Proceedings of the 28th International Conference on High-energy Physics (ICHEP 96), Warsaw, Poland, 25-31 Jul 1996, p. 143, Editors Z. Ajduk and A. K. Wrobblewski, hep-ex/9701014.
[14] The B_S lifetime reported here has already been published previously in [9].
[15] CDF Collaboration, F. Abe *et al.*, Nucl. Inst. Meth. A **271**, 387 (1988).
[16] D. Amidei *et al.*, Nucl. Inst. Meth. A **350**, 73 (1994).
[17] Throughout this paper transverse refers to the plane perpendicular to the proton beam.
[18] CDF Collaboration, F. Abe *et al.*, Phys. Rev. Lett. **79**, 578 (1997).
[19] G.W. Foster *et. al.*, Nucl. Inst. Meth. A **269**, 93 (1988).
[20] Particle Data Group, Phys. Rev. D **54**, (1996).
[21] CDF Collaboration, F. Abe *et al.*, Phys. Rev. D **53**, 3496, (1996).
[22] E. D. Courant and H. S. Snyder, Ann. Phys. 3, 1 (1958); D. A. Edwards and M. J. Syphers, "An Introduction to the Physics of High Energy Particle Accelerators", John Wiley and Sons, NY, 1993.
[23] G. Jackson, Editor, "Fermilab Recycler Ring Technical Design Report", FERMILAB-TM-1981.
[24] P. Nason, S. Dawson, R. K. Ellis, Nucl. Phys. B **327**, 49 (1989).
[25] C. Peterson *et al.*, Phys. Rev. D **27**, 105 (1983).
[26] CDF Collaboration, F. Abe *et al.*, Phys. Rev. D **54**, 6596 (1996).
[27] P. Avery, K. Read, and G. Tahern, Cornell Internal Note CSN-212, 1985 (unpublished).
[28] For current measurements of inclusive and exclusive $B \to J/\psi X$ decays see: CLEO Collaboration, R. Balest *et al.*, Phys. Rev. D **52**, 2661 (1995); CLEO Collaboration, J. Alexander *et al.*, Phys. Lett. B **341**, 435 (1995); CLEO Collaboration, M. S. Alam *et al.*, Phys. Rev. D **50**, 43 (1994).
[29] J. Chrin, Z. Phys. C **36**, 163 (1987).
[30] CDF Collaboration, F. Abe *et al.*, Phys. Rev. Lett. **75**, 4358 (1995).
[31] CDF Collaboration, F. Abe *et al.*, Phys. Rev. D **55**, 1142 (1997).

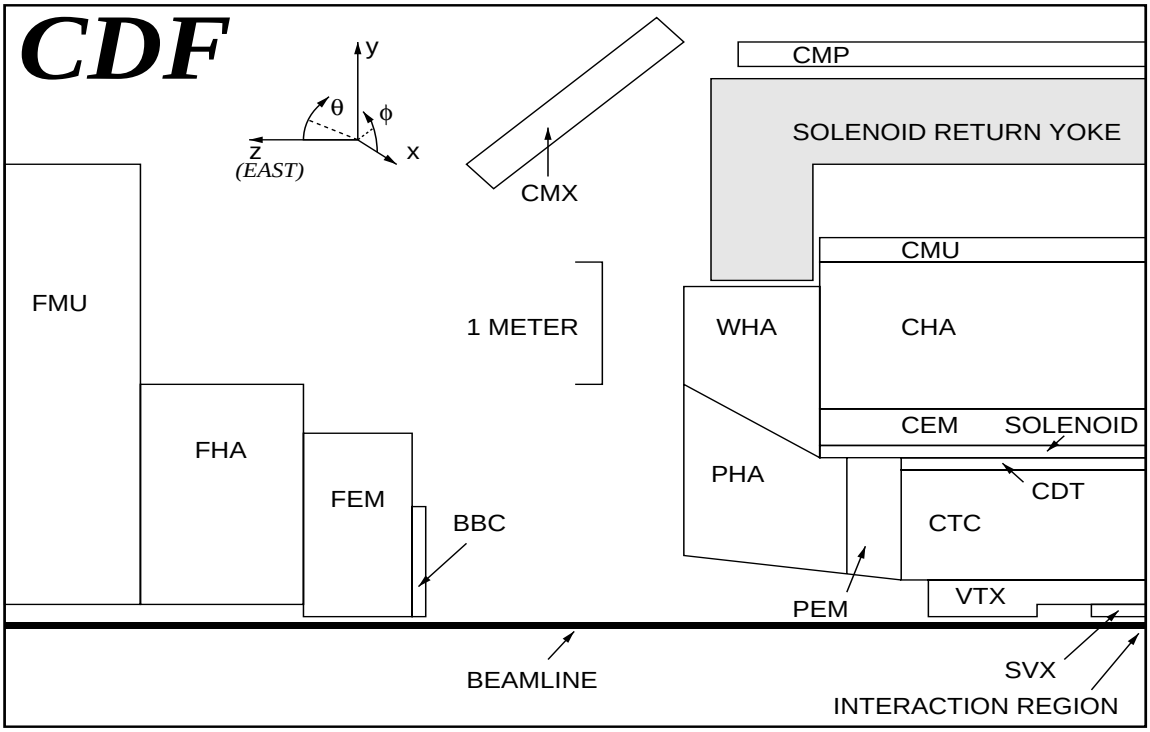

FIG. 1. Schematic quarter section of the central part of the CDF detector in Collider Run I, 1992-96.

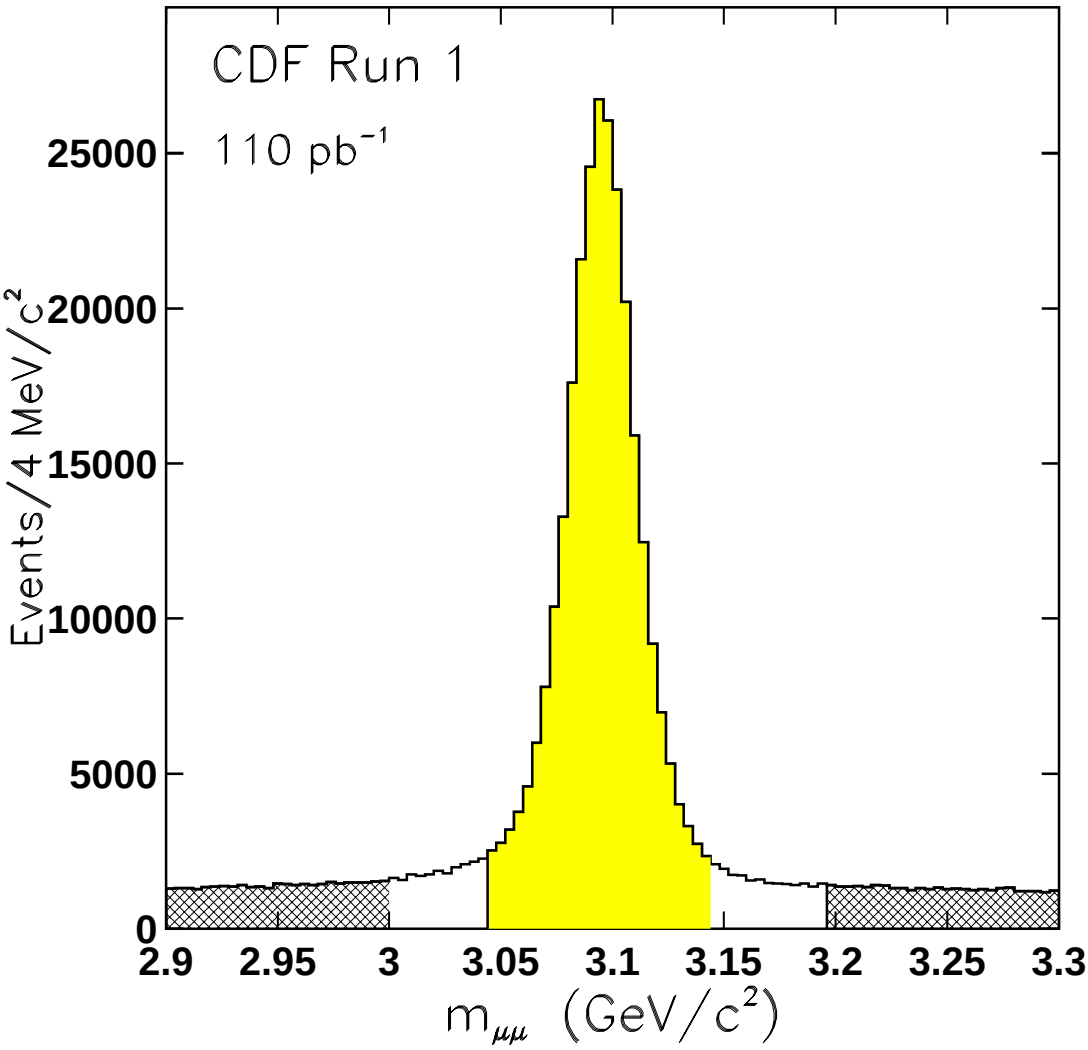

FIG. 2. Invariant mass distribution of oppositely charged muon pairs after selection cuts. Both muons were reconstructed in the SVX. A signal of 243,000±540 J/ψ candidates over a background of 34,000±130 events is observed. The width of the J/ψ mass peak is 16 MeV/c^2. The center area indicates the J/ψ signal region and the cross-hatched area shows the sideband regions used in the average lifetime measurement.

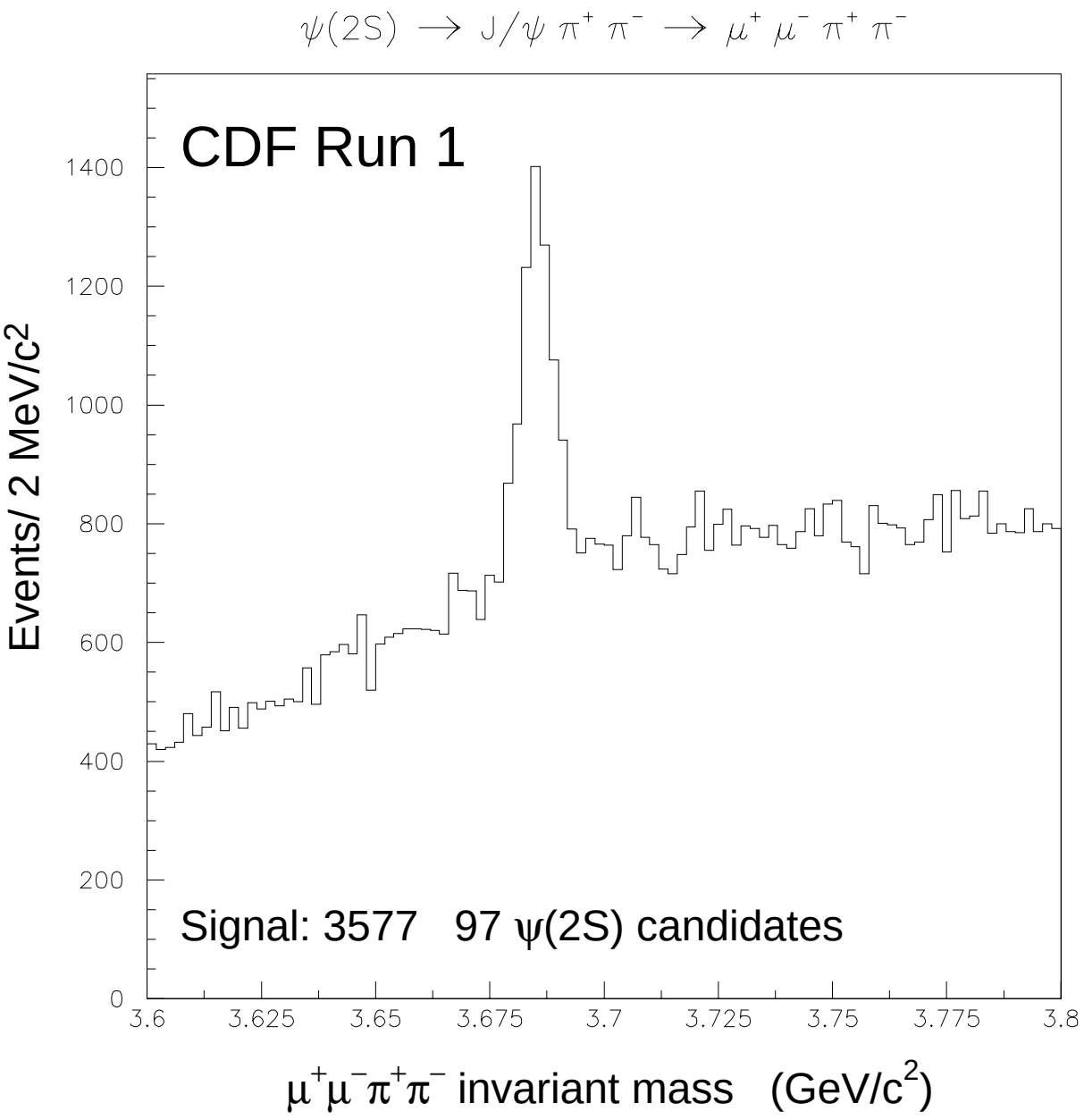

FIG. 3. Invariant mass distribution of $\psi(2S)$ candidates, we observe 3577 ± 97 $\psi(2S)$ candidates after background subtraction.

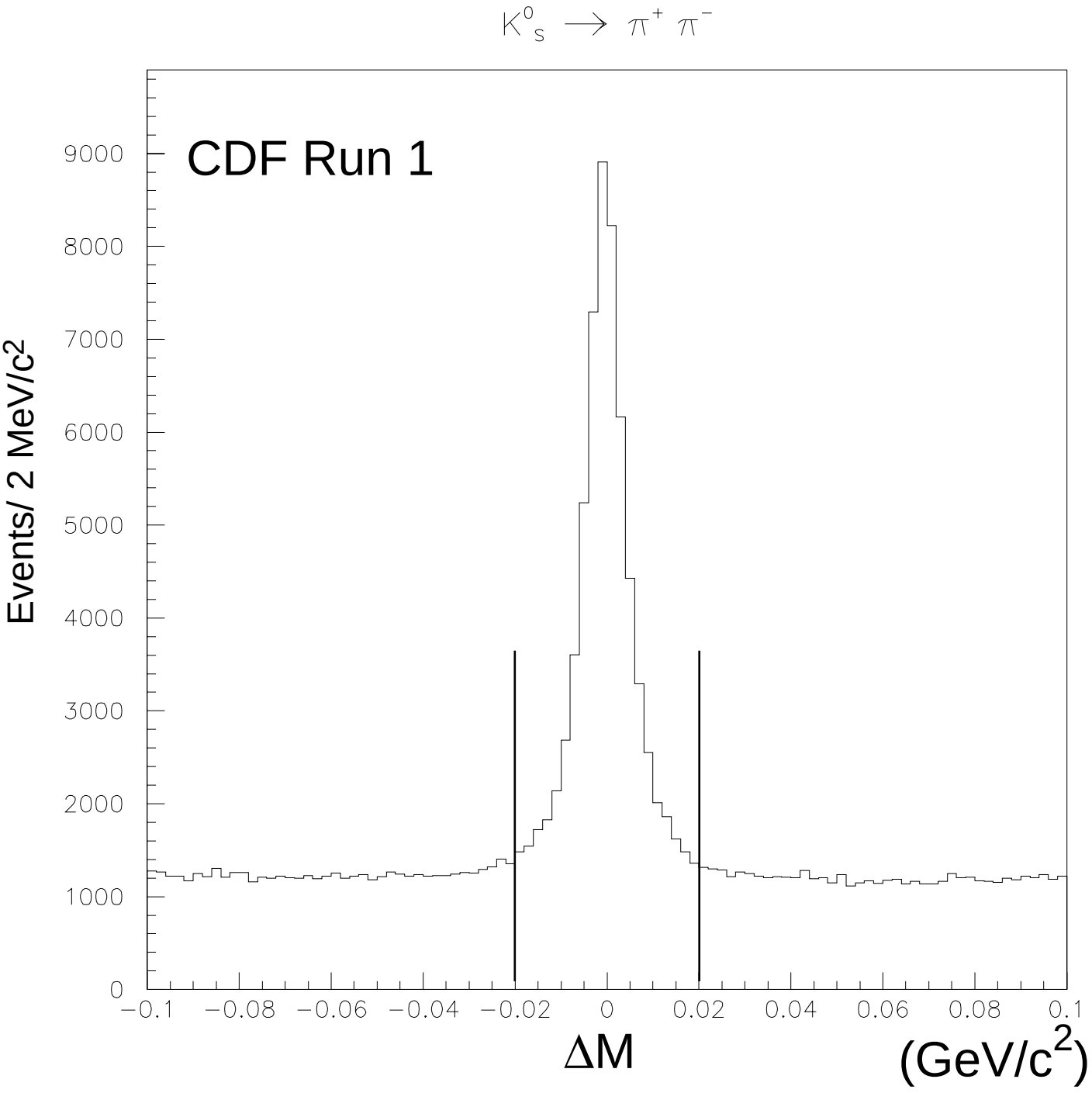

FIG. 4. Invariant mass distribution of K_s^o candidates, we observe 42,600 candidates, after background subtraction, in the J/ψ sample. ΔM is the mass difference between the world average mass value and the measured mass. The lines mark the mass window we used to define K_s^o candidates.

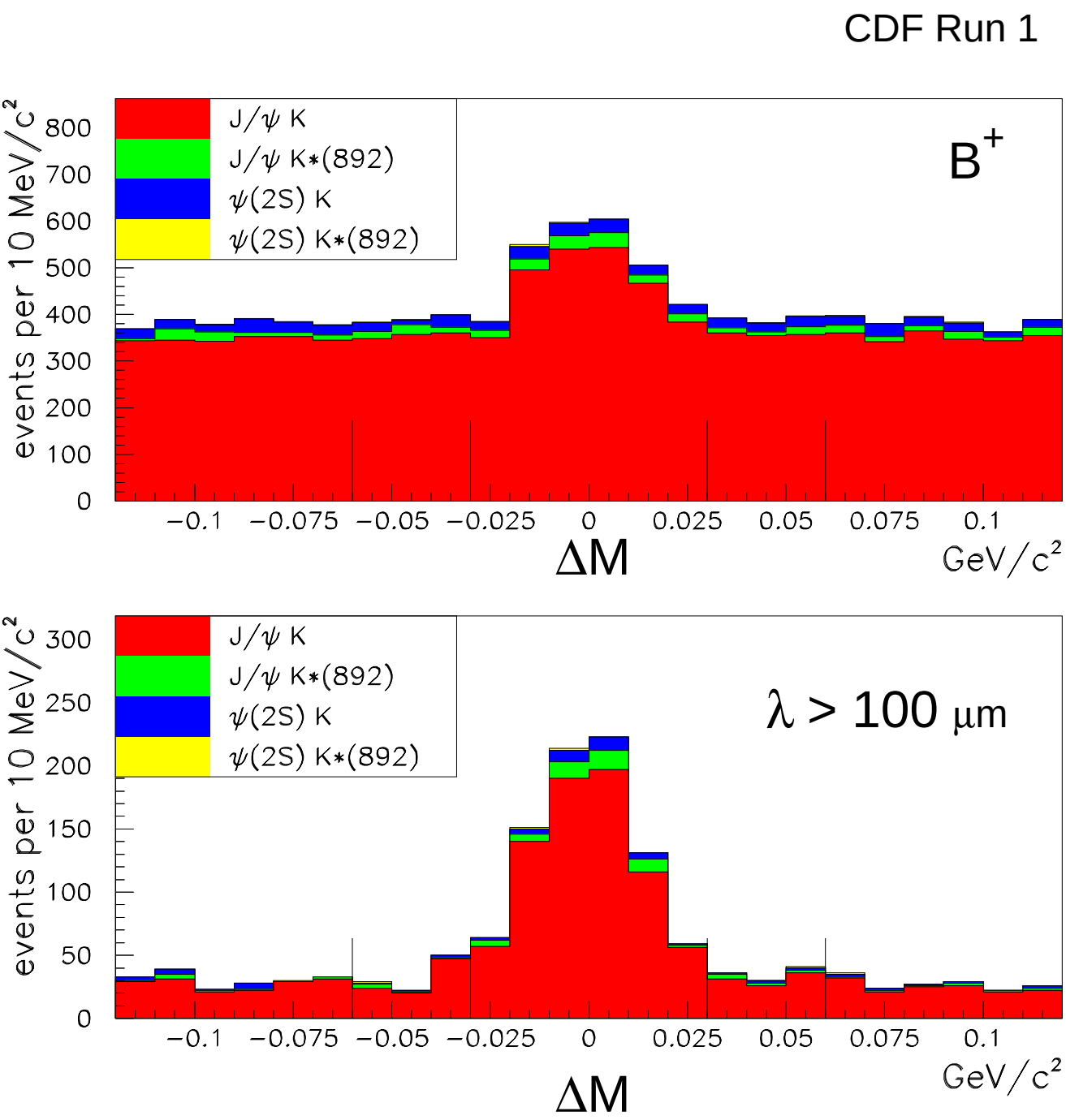

FIG. 5. Invariant mass distributions of reconstructed B^+ meson candidates. ΔM is the mass difference between the world average and the measured mass. All the events passing the cuts described in the text are shown in the upper plot. The distribution for events with the proper decay length $\lambda > 100$ μm is shown in the lower plot. In the fit to the lifetime, the peak region is defined as the six central bins and the sideband regions are defined as the six leftmost and six rightmost bins.

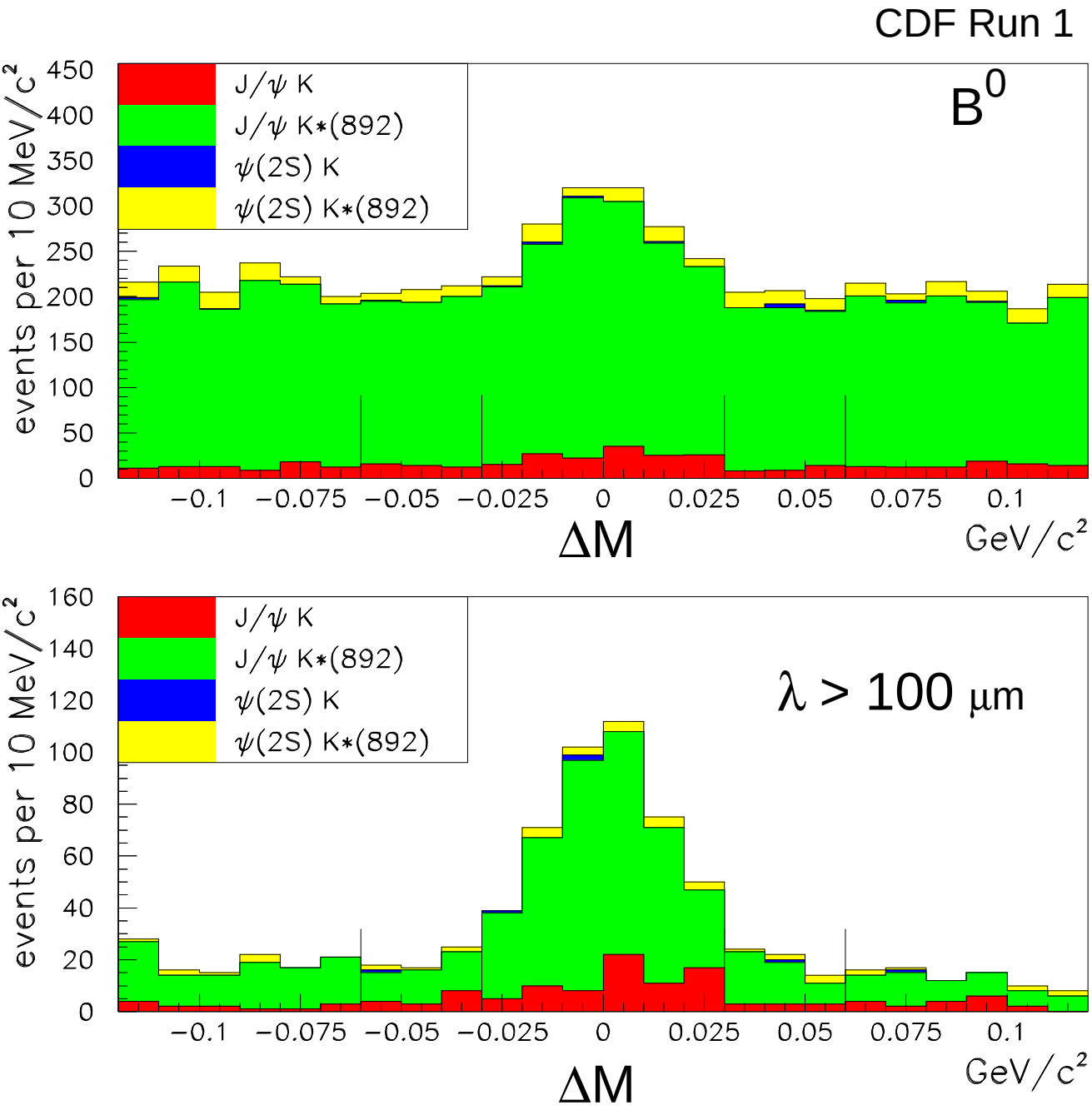

FIG. 6. Invariant mass distributions of reconstructed B^0 mesons. ΔM is the mass difference between the world average and the measured mass. All the events passing the cuts described in the text are shown in the upper plot. The distribution for events with the proper decay length $\lambda > 100$ μm is shown in the lower plot. In the fit to the lifetime, the peak region is defined as the six central bins and the sideband regions are defined as the six leftmost and six rightmost bins.

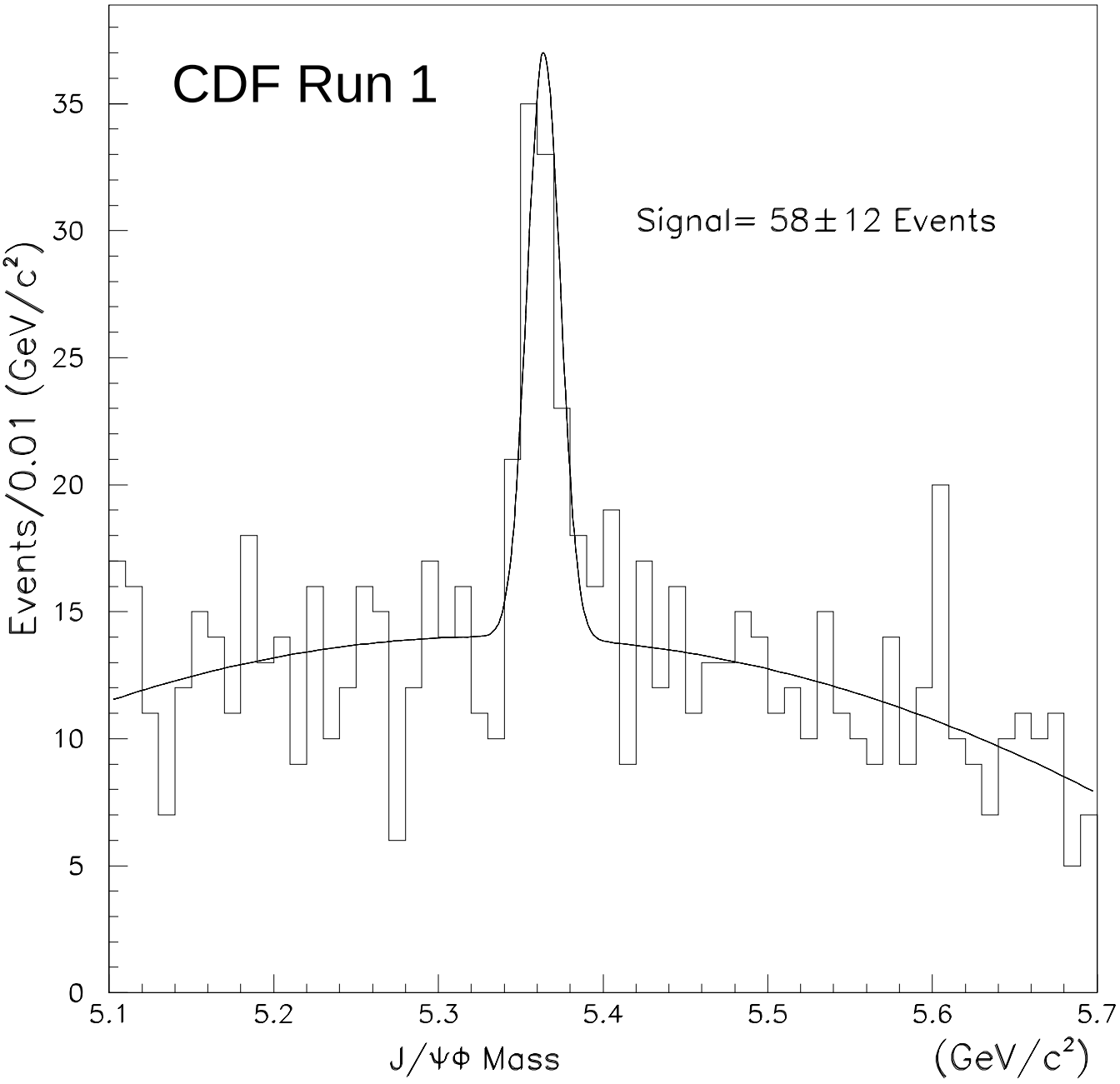

FIG. 7. The invariant mass distribution of B_s^0 candidates for $p_T(\phi) > 2$ GeV/c is shown fitted to a Gaussian plus a polynomial background. The typical uncertainty on the reconstructed mass was 0.01 GeV/c^2.

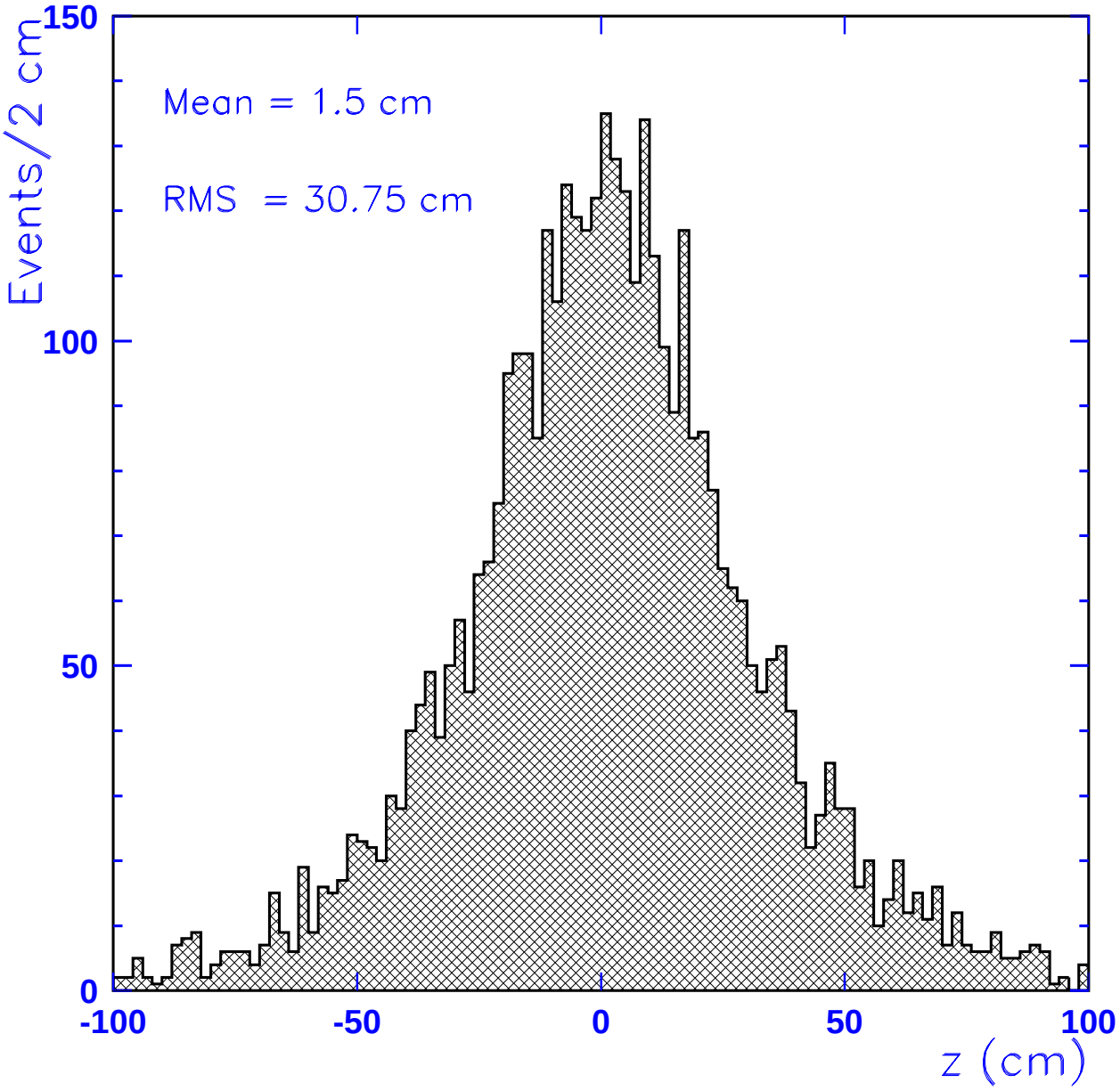

FIG. 8. Distribution of primary vertices along the proton direction (z) for a typical data acquisition run.

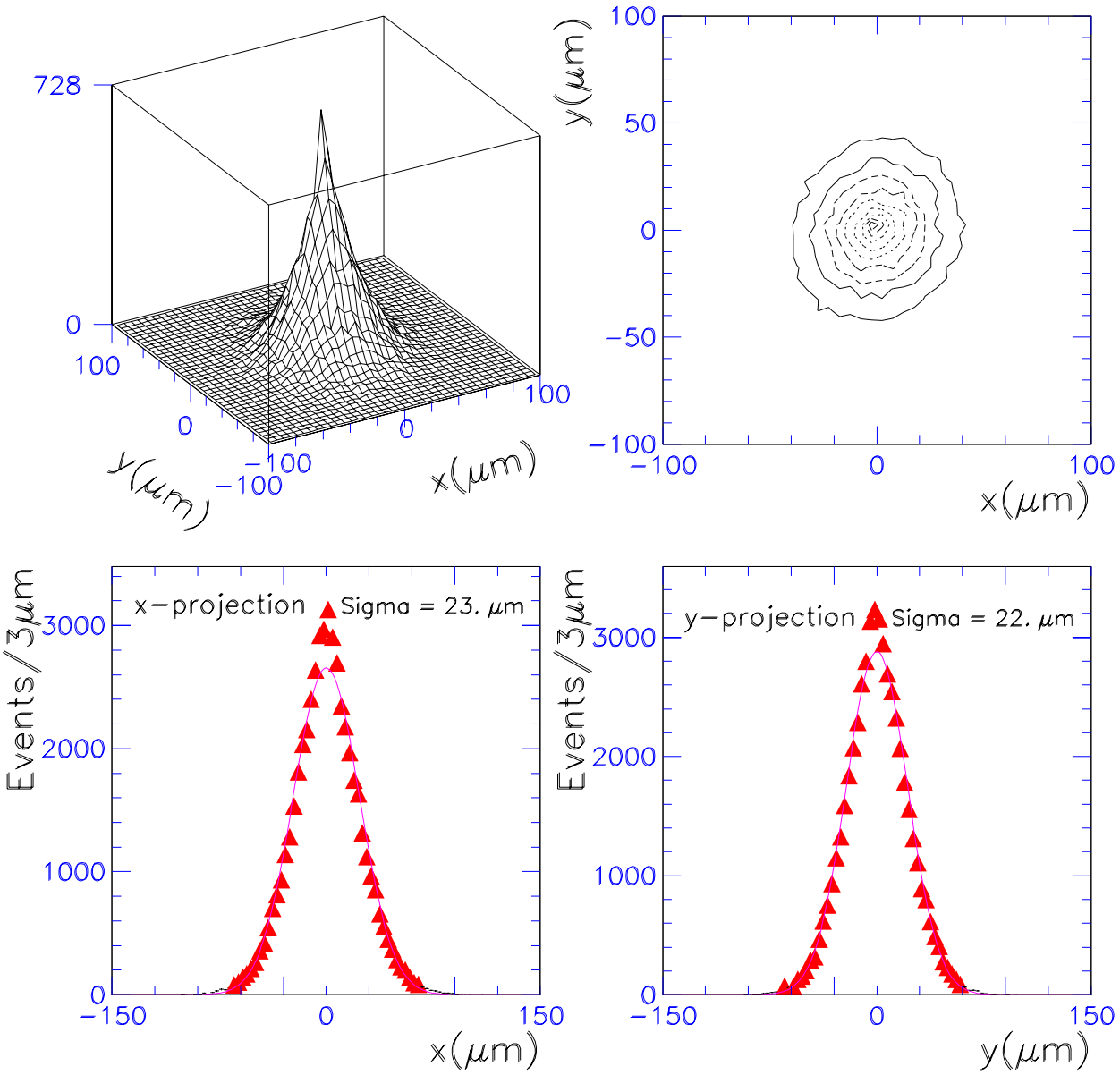

FIG. 9. The two dimensional distribution of the beam spot for a typical data acquisition run during the 94-95 running period is shown in the upper two plots . The x and y projection, respectively are shown in the lower two plots. Typically, the beam was roughly circular and had a Gaussian profile. For this run the σ was 23 μm in x and 22 μm in y. These values are the average over the length of the SVX detector.

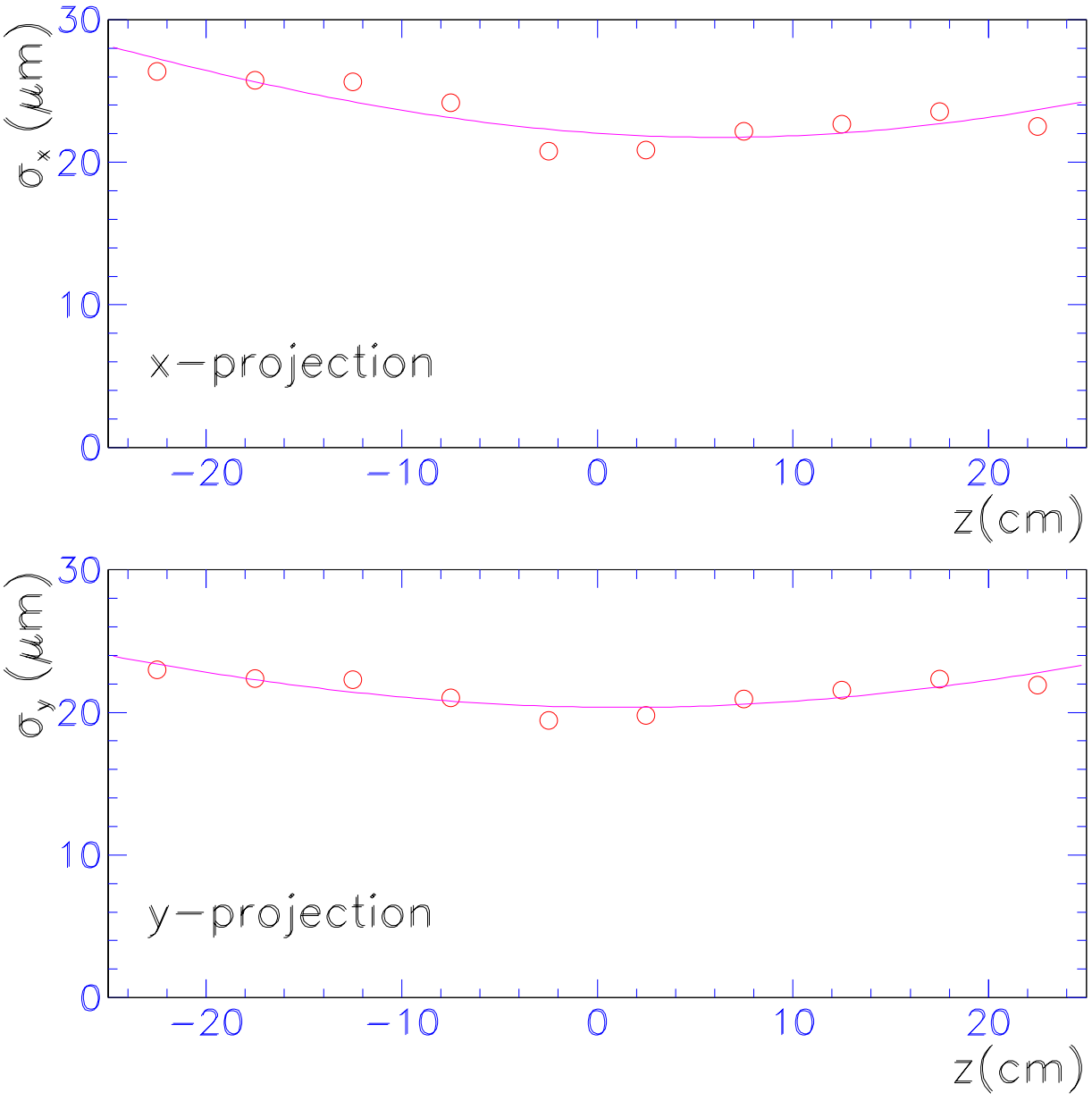

FIG. 10. Width σ of the beam in x and y as a function of z with the fitted functions superimposed.

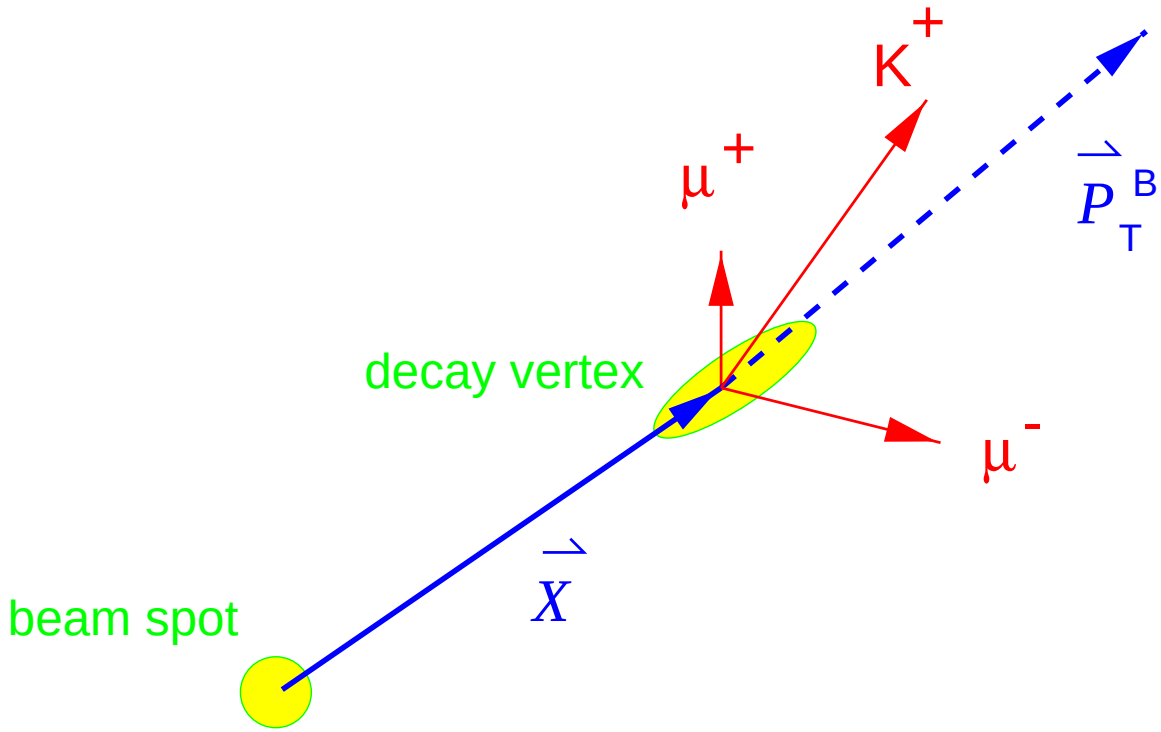

FIG. 11. Definition of the transverse decay length L_{xy}.

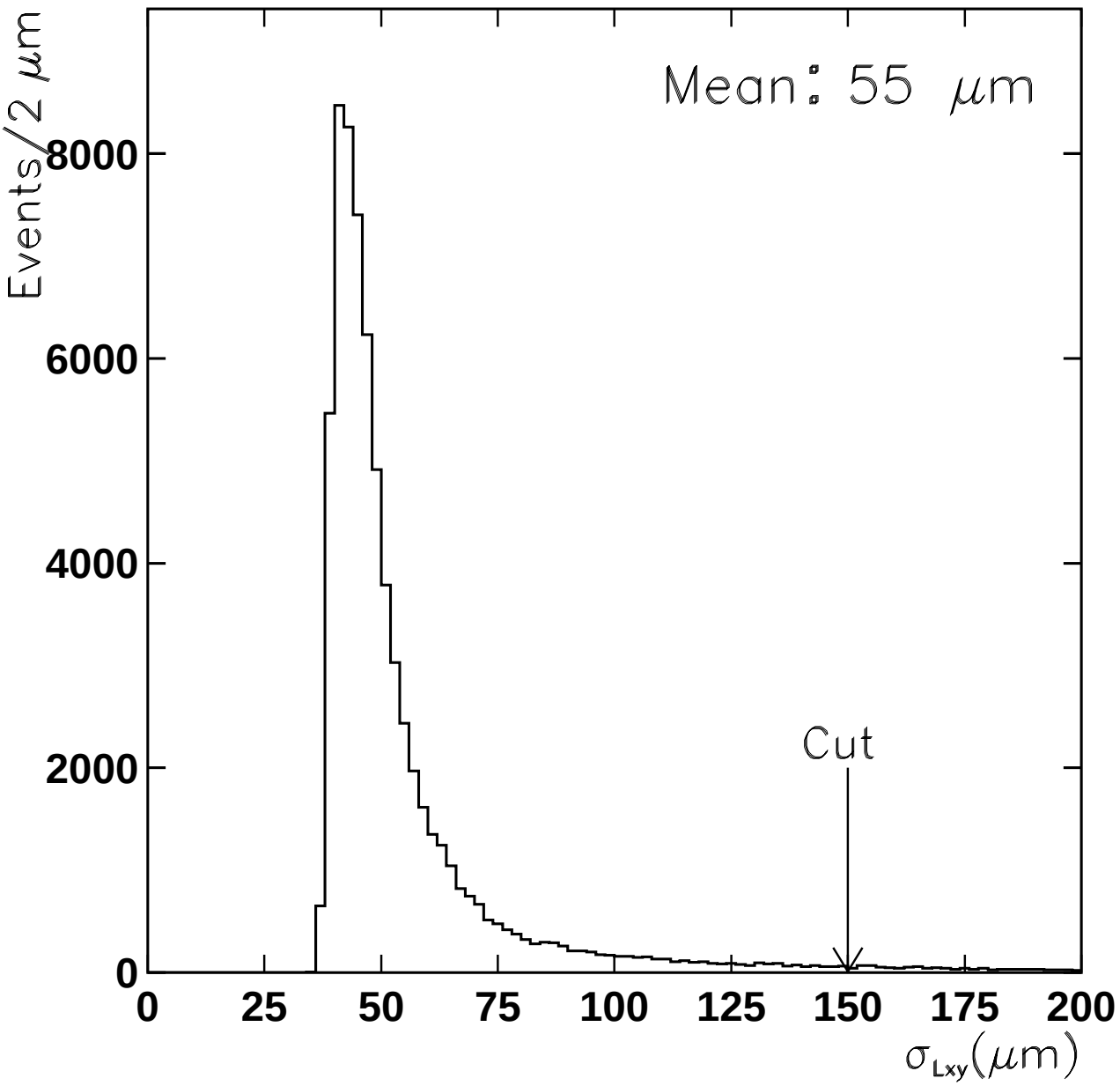

FIG. 12. Distribution of the calculated uncertainty $\sigma_{L_{xy}}$ of the transverse decay length for J/ψ events.

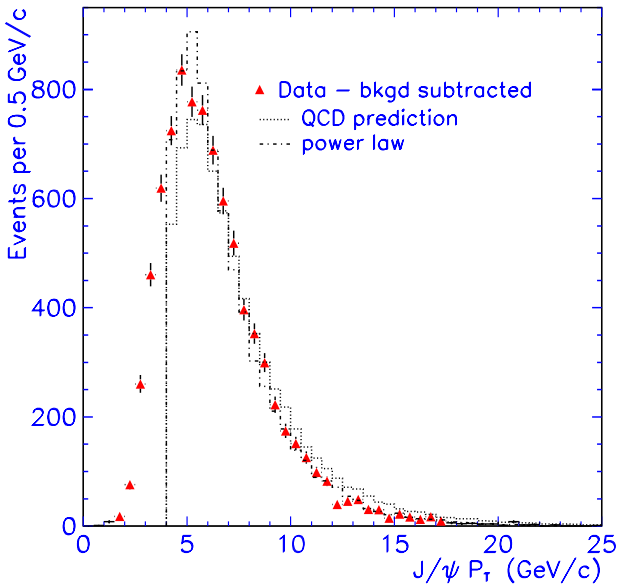

FIG. 13. The transverse momentum of J/ψ mesons for NDE, power law and data. The data is shown before the $P_T^{\psi} > 4.0$ GeV/c cut. The data distribution was background subtracted, and the proper decay length was required to be larger than 200 μm to ensure that all J/ψ originate from b-decays. The number of Monte Carlo events were normalized to the number of data events with $P_T^{\psi} > 4.0$ GeV/c.

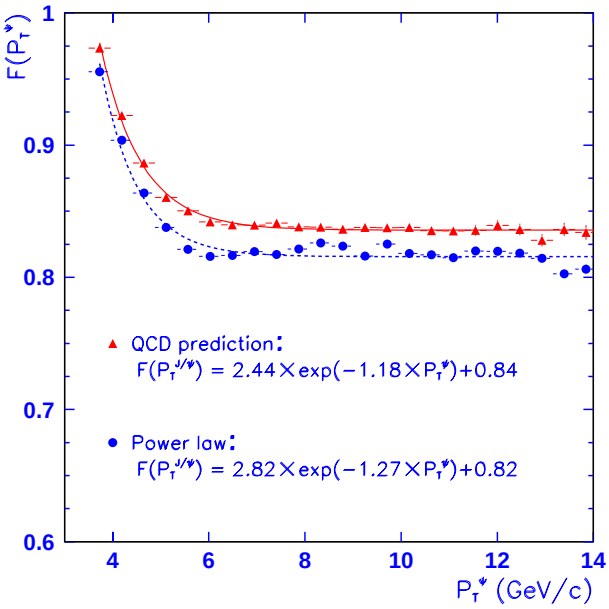

FIG. 14. The correction factor $F(p_T^{\psi})$ for the QCD prediction and for a power law.

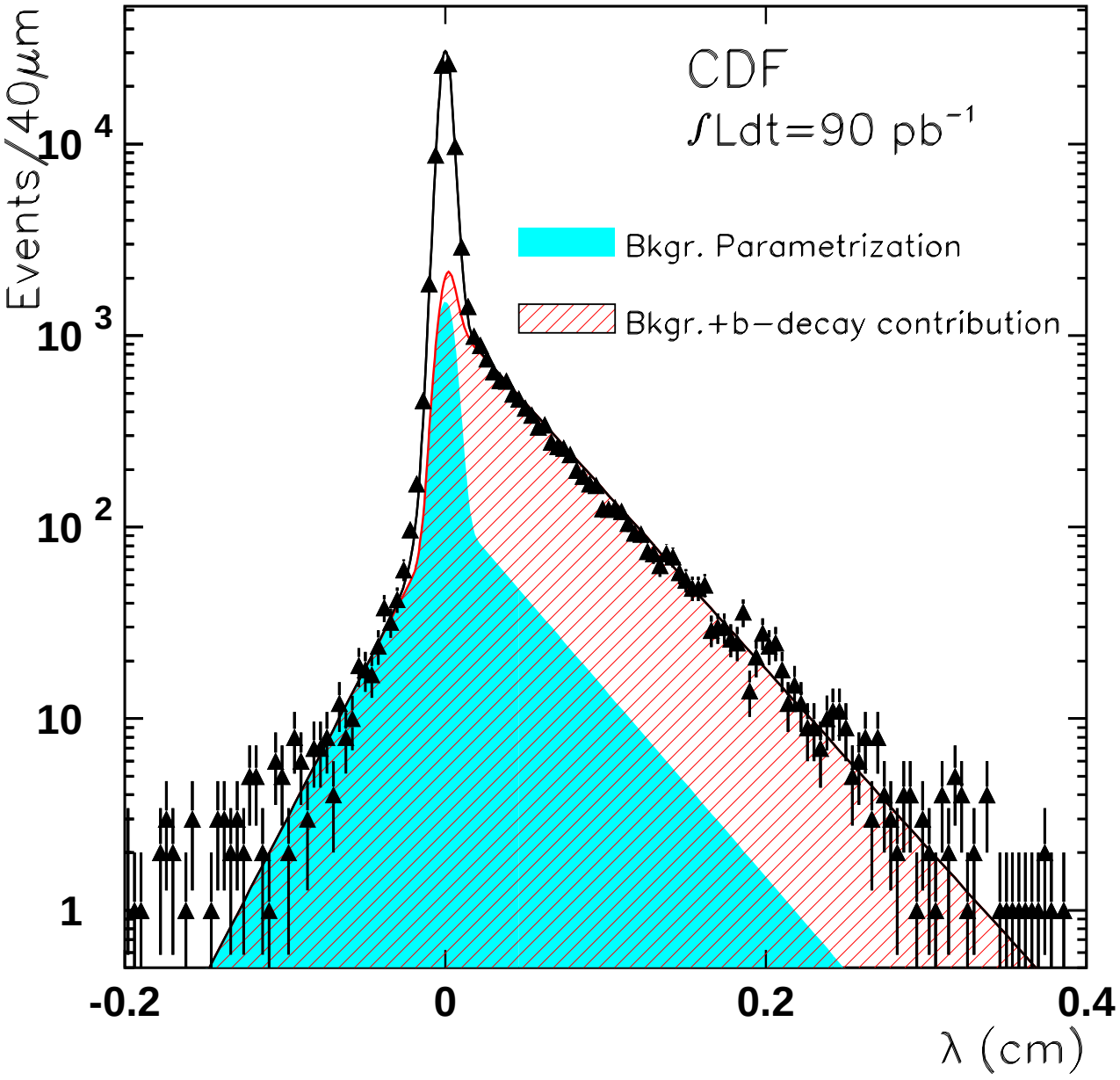

FIG. 15. The pseudo proper decay length distribution of the signal region with the unbinned likelihood fit superimposed. The plot shows the contributions from the three different sources. The distribution of background events as obtained from the fit to the λ distribution of the J/ψ sidebands, the sum of the background distribution and the Gaussian function convoluted with the exponential from b-decay and finally the remaining Gaussian centered at 0 (unshaded area) which is due to decays of prompt J/ψ's.

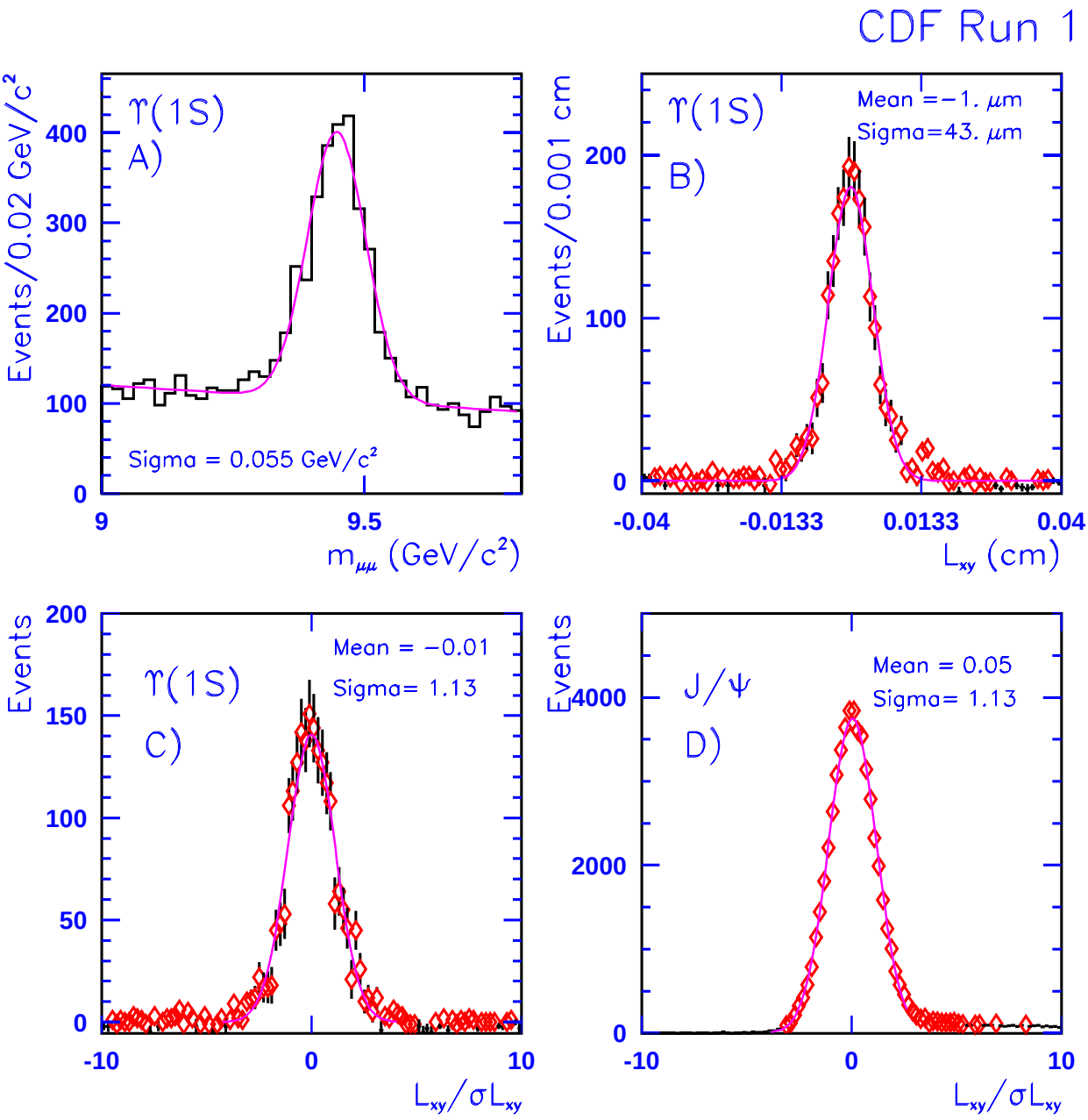

FIG. 16. (A) The dimuon invariant mass spectrum in the $\Upsilon(1S)$ region. Both tracks were required to be reconstructed in the SVX. The mass resolution is 0.055 GeV/c^2. (B) The L_{xy} distribution of $\Upsilon(1S)$ candidates after sideband subtraction. The shape is Gaussian with a mean consistent with zero and a resolution of 43 μm. (C) The $L_{xy}/\sigma_{L_{xy}}$ distribution after sideband subtraction. A fit of a Gaussian function to the distribution yielded a sigma of 1.13 indicating that the calculated error σL_{xy} was underestimated by 13%. (D) $L_{xy}/\sigma_{L_{xy}}$ distribution for the J/ψ sample. A fit to the prompt part of the distribution indicated that the error was underestimated by 13%.

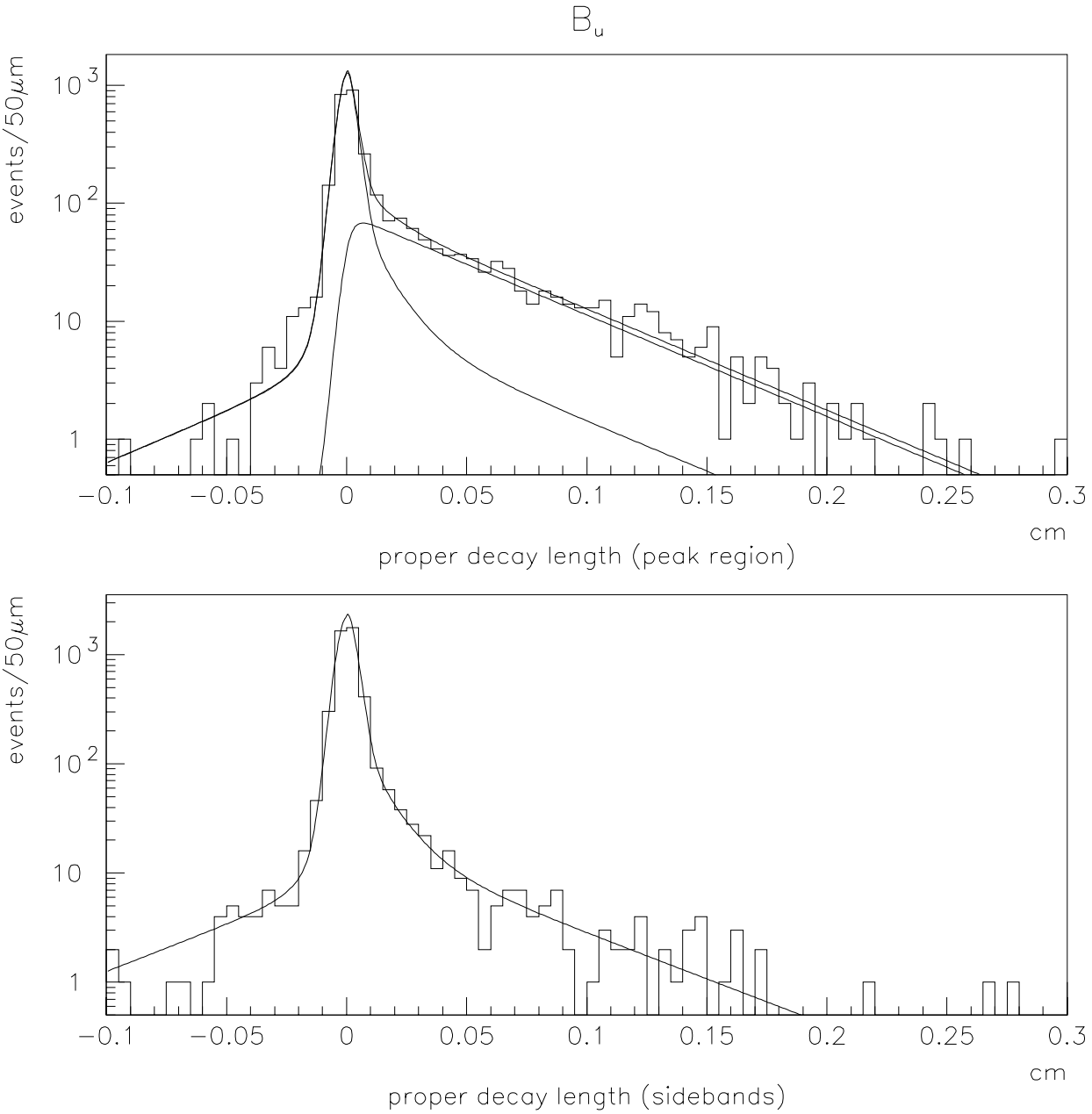

FIG. 17. The proper decay length distribution for all reconstructed B^+ mesons. The upper (lower) histogram shows the peak (sideband) region distribution. The first (last) bin of each histogram gives the number of underflow (overflow) events. The superimposed curves are the contributions from the signal, the background and their sum as determined by the likelihood fit described in the text.

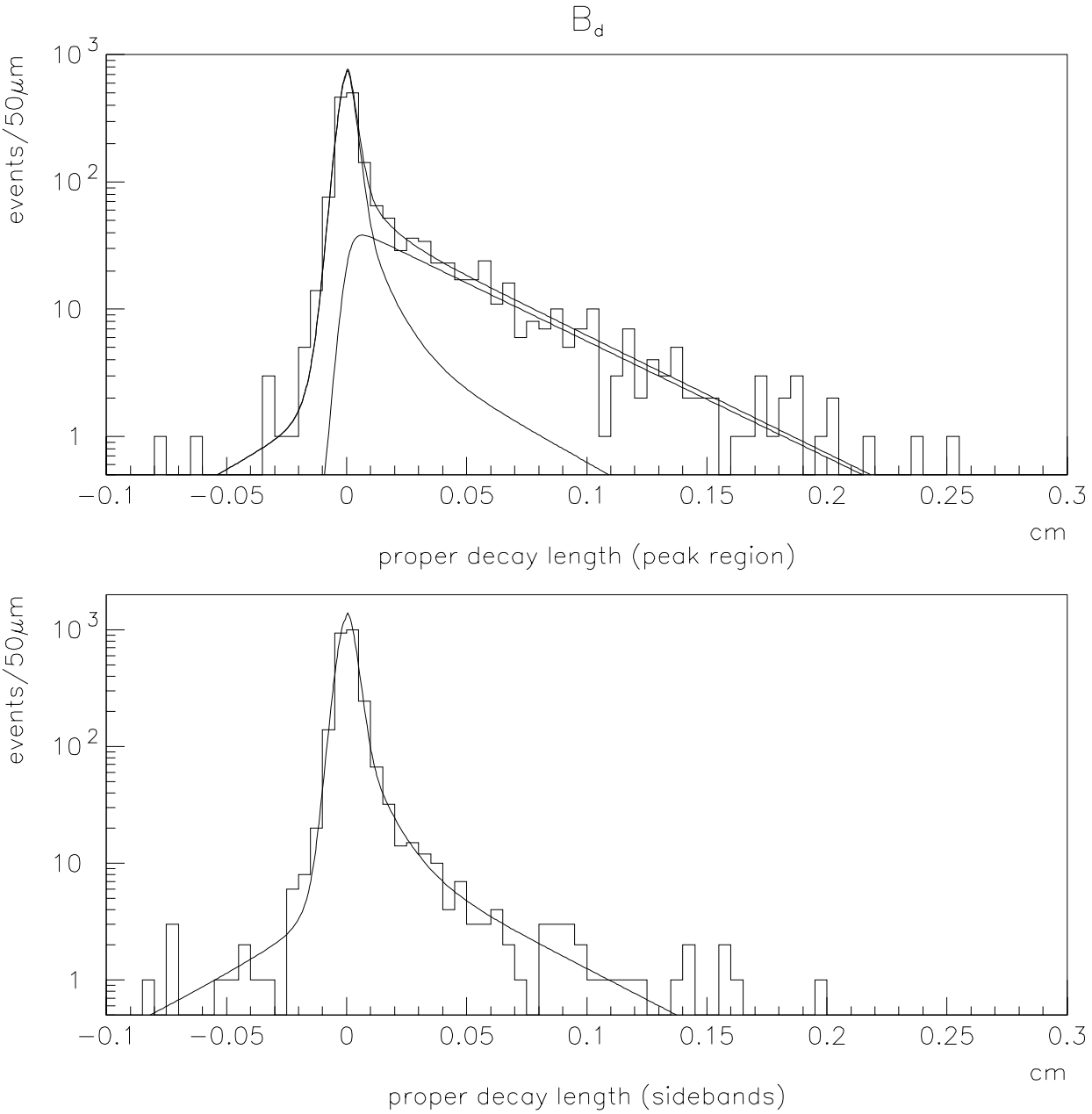

FIG. 18. The proper decay length distribution for all reconstructed B^0 mesons. The peak (sideband) region distribution is shown in the upper (lower) histogram. The first (last) bin of each histogram gives the number of underflow (overflow) events. The superimposed curves are the contributions from the signal, the background and their sum as determined by the likelihood fit described in the text.

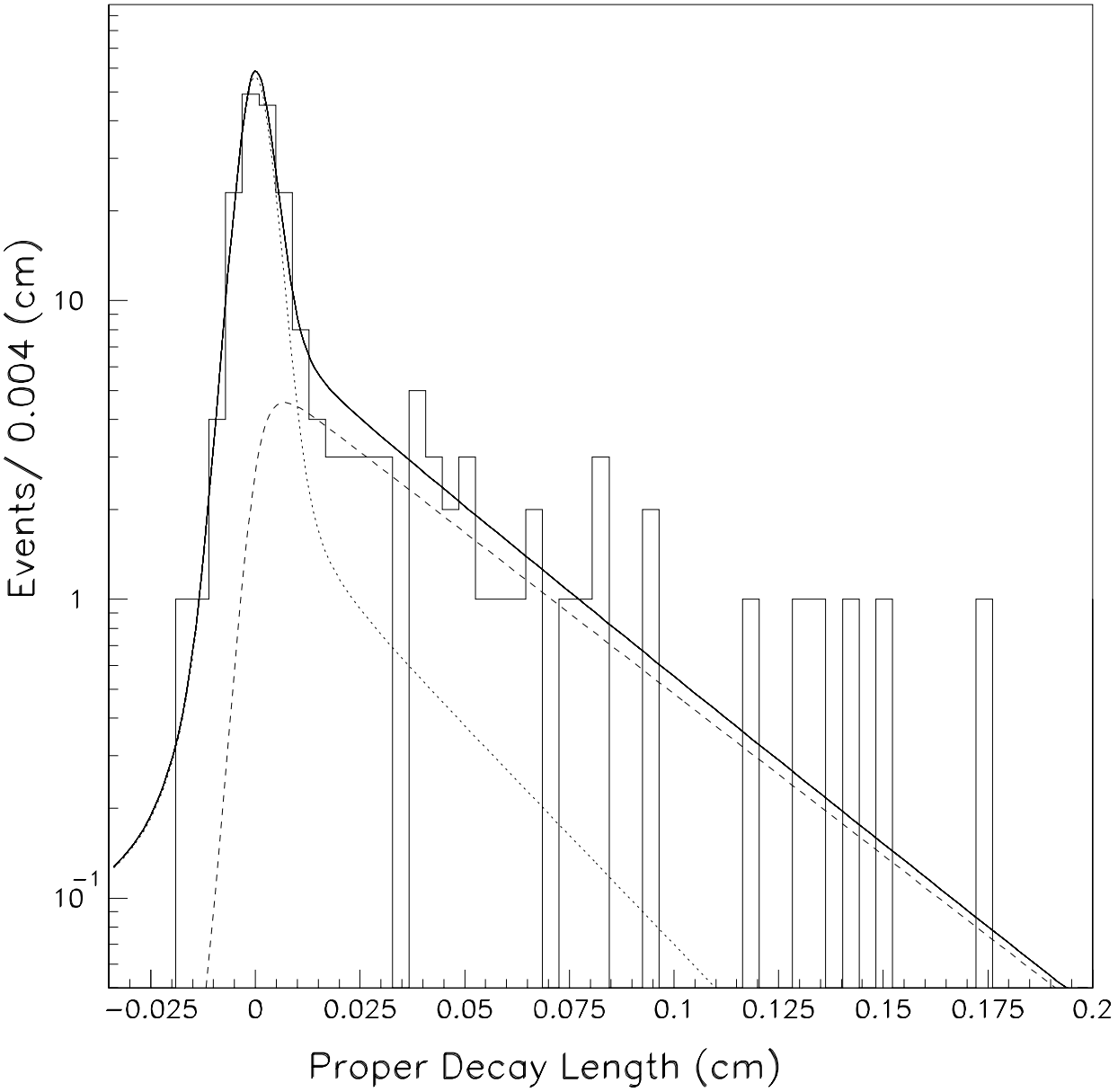

FIG. 19. The proper decay length distribution of the B_s^0 for events selected within ± 0.05 GeV/c^2 of the B_s^0 fitted mass. The results of the lifetime fit are shown, signal (dashed line), background (dotted line), and the sum of the two (solid line). The typical error on the calculated proper decay length was 40 μm.

Parameter	Fit Value
x: emittance	$(1.10 \pm 0.07) \times 10^{-9}$ m
x: β^*	0.40 ± 0.03 m
x: z_0	0.06 ± 0.01 m
y: emittance	$(1.06 \pm 0.06) \times 10^{-9}$ m
y: β^*	0.39 ± 0.03 m
y: z_0	0.003 ± 0.007 m

TABLE I. Results of the fit to the width of the beam as a function of z using the x and y projections for one data acquisition run. Errors are statistical only.

Parameter (sideband region)		Value	Uncertainty
f^+	[%]	27	$\pm$ 0.6
λ^+	[μm]	429	$\pm$ 11
f^-	[%]	11.3	$\pm$ 0.5
λ^-	[μm]	231	$\pm$ 10
Parameter (signal region)		**Value**	**Uncertainty**
λ_B (corrected for fitting bias)	[μm]	460	$\pm$ 5
f_B	[%]	17.7	$\pm$ 0.2
s		1.15	$\pm$ 0.05

TABLE II. Parameters of likelihood fit to sideband and signal regions.

Systematic	Uncertainty [%]	
NDE versus Power Law	-1.4	$+1.4$
ϵ (Peterson) 0.004-0.008	-0.6	$+1.3$
L2 trigger	-0.1	$+0.1$
B_s^0 fraction	-0.3	$+0.3$
Polarization	-1.0	$+1.0$
Λ_b production	-0.2	$+0.2$
Total	-1.9	$+2.2$

TABLE III. Systematic errors due to production and decay kinematics in %.

Systematic	Uncertainty [%]	
Production and Decay Kinematics	-1.9	$+2.2$
Background Parametrization	-0.4	$+0.4$
Length Scale (Alignment)	-0.3	$+0.3$
Fitting Procedure Bias	-0.5	$+0.5$
Total	-2.0	$+2.3$

TABLE IV. Summary of systematic errors for the inclusive lifetime measurement.

Parameter		B^+	B^0
λ	[μm]	505 ± 21	475 ± 27
α	[%]	26.5 ± 0.9	25.7 ± 1.3
events	[events]	824 ± 36	436 ± 27
f_1^-	[%]	1.95 ± 0.20	1.20 ± 0.22
f_1^+	[%]	4.43 ± 0.65	4.69 ± 0.93
f_2	[%]	7.97 ± 0.87	9.99 ± 1.30
λ_1	[μm]	516 ± 39	409 ± 48
λ_2	[μm]	106 ± 15	87 ± 13

TABLE V. Fit parameters for the B^+ and B^0 lifetime measurement.

Systematic	B^+	B^0
Scale factor	±0.2 %	±0.2 %
non-Gaussian tails	±1.2 %	±1.1 %
Fitting Procedure Bias	±0.2 %	±0.4 %
Length Scale	±0.3 %	±0.3 %
Total	±1.3 %	±1.2 %

TABLE VI. Summary of systematic errors for the B^+ and B^0 lifetime measurement.

Parameter		Value	Uncertainty
$\lambda_{B_s^0} = c\tau(B_s^0)$	[μm]	402	$^{+69}_{-57}$
f_s	[%]	7.2	± 1.1
f^+	[%]	10.3	± 1.6
λ^+	[μm]	297	± 47
f^-	[%]	14.9	± 0.51
λ^-	[μm]	639	± 214
s		1.09	± 0.04
$M_{B_s^0}$	[GeV/c^2]	5.364	± 0.002
p_1	[(GeV/c^2)$^{-2}$]	-0.368	± 0.379
p_2	[(GeV/c^2)$^{-3}$]	-6.176	± 2.207

TABLE VII. Fit parameters for the B_s^0 mass and lifetime distributions with a cut of $p_T(\phi) > 2$ GeV/c. The range in mass was 5.1–5.7 GeV/c^2. The total number of events was 804.

Systematic	Uncertainty [%]
Background parametrization	3.5
Fitting Procedure Bias	0.5
SVX Length Scale	0.3
Total	3.5

TABLE VIII. Summary of systematic uncertainties for the B_s^0 lifetime measurement.